Spring 5-7-2021

Gait Rehabilitation Using Biomechanics and Exoskeletons

Jacob Bloom
jbloom890@gmail.com

GAIT REHABILITATION USING BIOMECHANICS AND EXOSKELETONS

By

Jacob Bloom

B.S. University of Maine, 2019

A THESIS

Submitted in Partial Fulfillment of the

Requirements for the Degree of

Master of Science

(in Mechanical Engineering)

The Graduate School

The University of Maine

May 2021

Advisory Committee:

Dr. Babak Hejrati, Assistant Professor of Mechanical Engineering, Advisor

Dr. Mohsen Shahinpoor, Professor of Mechanical Engineering

Dr. Andrew Goupee, Associate Professor of Mechanical Engineering

GAIT REHABILITATION USING BIOMECHANICS AND EXOSKELETONS

By Jacob Bloom

Thesis Advisor: Dr. Hejrati

An Abstract of the Thesis Presented
in Partial Fulfillment of the Requirements for the
Degree of Master of Science
(in Mechanical Engineering)
May 2021

A healthy gait is often taken for granted when walking. However, if a stroke, spinal cord injury (SCI), or traumatic event occurs the ability to walk may be lost. In order to relearn how to walk, gait rehabilitation is required. Including arm swing in gait rehabilitation has been shown to help in this process. This thesis presents two tasks to investigate the mechanics of arm swing and ways to provide assistance to induce arm swing in gait rehabilitation.

The firsts task completed was a study on the effects of forearm movement during gait. Twelve healthy subjects walked under three conditions at two self selected speeds. The first condition observed was natural walking, the second condition the subjects wore an artificial forearm with their forearms restricted, and the third condition the subjects' forearms were restricted without the artificial forearm. It was observed that the the lower extremities' range of motion and spatiotemporal parameters did not change between conditions. However when the subjects wore the artificial forearm, significant decreases were observed in the shoulders, trunk, interlimb coordination, and shoulder trunk correlations. In addition, increases in muscle activity also occurred in the biceps, trapezius, and posterior deltoids during the second condition. The amount of energy exerted also increased when wearing the artificial forearm, but not significantly. Only restraining the forearms mainly

affected shoulder rotation at the subjects' normal walking speed. These results indicate that the body actively controls forearm movements during walking to mitigate unwanted movements. It does this by reducing shoulder and trunk rotation.

The second task was the design and validation of a distally located upper extremity exoskeleton to assist with arm swing during gait rehabilitation. This exoskeleton utilizes a hybrid double parallel linkage (DPL) that allows the exoskeleton to mimic the work-space of a healthy shoulder. The motor is distally located from the shoulder and located on a ALICE backpack. This provides several ergonomic benefits such as reducing the weight on the wearer's arm. The torque is transferred from the motor to the arm through a pulley system. The exoskeleton's ability to generate arm swing was validated on a passive dummy arm. The exoskeleton was tested under two conditions. The first condition was in-plane arm swing, which simulated motion strictly in the sagittal plane. The second condition was out-of-plane arm swing to simulate arm swing when the shoulder is internally rotated. Each condition was tested at frequencies of 0.67, 0.80, 1.10 Hz. It was observed that the exoskeleton can generate highly correlated movements in the passive arm at each of the tested frequencies with low time lags. In addition the exoskeleton was also tested on two subjects. Similarly, arm movements were highly coordinated to motor movements. Based on these results, this exoskeleton design has the potential to aid in gait rehabilitation.

ACKNOWLEDGEMENTS

The thesis presented is a culmination of two years of rigorous research, experimentation, and data analysis. I would like to thank my advisor, Dr. Babak Hejrati, for mentoring me throughout this experience. Much of my success would not have been possible without his guidance. In addition, I would like to thank my friends and family for supporting me throughout my graduate career. At times this journey was daunting and discouraging, and it would not have been possible without their encouragement and support.

TABLE OF CONTENTS

LIST OF TABLES

LIST OF FIGURES

CHAPTER 1

INTRODUCTION

Arm swing is an important component to maintain a healthy walking gait. The use of arm swing during gait has been shown to reduce energy consumption [4], improve balance [5], and increase rotational stability [6]. However, people can lose the ability to coordinate their upper extremities with their lower extremities due to a stroke, spinal cord injury (SCI), or traumatic injury. Gait rehabilitation is then needed. It has been shown that the inclusion of arm swing for gait rehabilitation helps improve the interlimb neural coupling which activates lower limb muscle activity [7, 8]. Kaupp et al. [9] further proved that cyclic arm training improved the coordination between muscles and overall strength of upper and lower extremities. Recently, robotic devices are being developed to aid in upper extremity rehabilitation. The use of robotic devices in rehabilitation helps physical therapists provide more consistent treatment [10]. The following sections in this chapter will further describe the components of arm swing and the different types of robots being used to help aid in rehabilitation.

1.1 Arm Swing in Gait Rehabilitation

Arm swing is often defined as the flexion and extension of the arm in the sagittal plane during walking. When being observed, shoulder angle is often the main kinematic variable of interest [11, 12]. As stated above, arm swing can be used to help in gait rehabilitation. Several studies have been performed to investigate the benefits of utilizing arm swing for patients with a spinal cord injury [13], Parkinson's disease [14, 15], and post stroke [16, 17, 18]. Changes in arm swing have been shown to produce changes to one's natural walking gait. De Graaf et al. [19] investigated the effects of changing arm swing amplitudes on gait. They observed that a decrease in arm swing amplitude reduced vertical angular momentum while an increase in arm swing amplitude caused an increase in energy

consumption. Wu et al. [11] determined that changes in arm swing significantly impacted dynamic stability. In addition, Pontzer et al. [20] studied how an arm is controlled during walking. It was noted that changes in upper extremities did not effect lower extremities.

To further understand the effects of arm swing, studies are being conducted to determine if arm swing is actively controlled or purely a passive movement. Pontzer et al. [20] theorize that arm swing is primarily a passive movement used to reduce head and torso rotation. However, Goudriaan et al. [21] dismisses this theory as they claim it takes muscle activity to increase arm swing amplitude and maintain out of phase movements with the legs. Both Canton et al. [22] and Kuhtz-Buschbeck et al.[23] further support the theory that there is an active component to arm swing. Kuhtz-Buschbeck et al. [23] observed an increase in EMG muscle activity when walking with out-of-phase arm swing. They suggest that arm swing is comprised of both passive and active components.

Although the effects of arm swing on gait has been studied rigorously, the effects of forearm movement during arm swing needs further investigation. There have been several studies that investigated the changes in gait when the elbow is locked and forearm movement is restricted during walking. Yegian et al. [24] studied changes that occur when the forearm is strictly bent and straight. They discovered that when the arms were bent, muscle torque in the elbow increased while muscle torque in the shoulder decreased. Oxygen consumption also increased by 11% when walking with bent arms. Koo et al. [25] determined that changes in the forearm effect gait parameters. These studies indicate that changes in forearm movements during walking effects gait.

1.2   Exoskeletons in Gait Rehabilitation

Robotic devices are being used in the field of rehabilitation. This is because these robotic devices have the capability to provide patients with more consistent and specialized treatment. There are several different characteristics for robotic devices in rehabilitation. Many robotic devices used for arm rehabilitation are fixed to the wall and are not portable

[26, 1, 27, 28, 29]. An example is the CAREX-7 robot [1] which is seen in figure 1.1. The CAREX-7 robot utilizes a cable system to help perform and aid in complex arm and hand movements. The CAREX-7 robot is fixed to the wall and requires the user to sit while it is being used. Although these fixed robotic devices show promising results for arm rehabilitation, this type of design is not suited for gait rehabilitation due to the subject being restricted to a fixed point or wall.

A robotic device needs to be able to be portable in order to aid in gait rehabilitation. This allows the wearer the ability to walk while the robotic device is being used. A robotic device that is worn is often considered an exoskeleton. When designing an exoskeleton for rehabilitation, the actuator is located either proximally [2, 30, 31] or distally [32, 33, 3, 34] away from the joint being rehabilitated. Figure 1.2a shows a design by Christensen et al.[2] where the motor is located proximally on the shoulder. This design utilizes a double parallel linkage (DPL) system to mimic the work-space of the user's shoulder. The use of
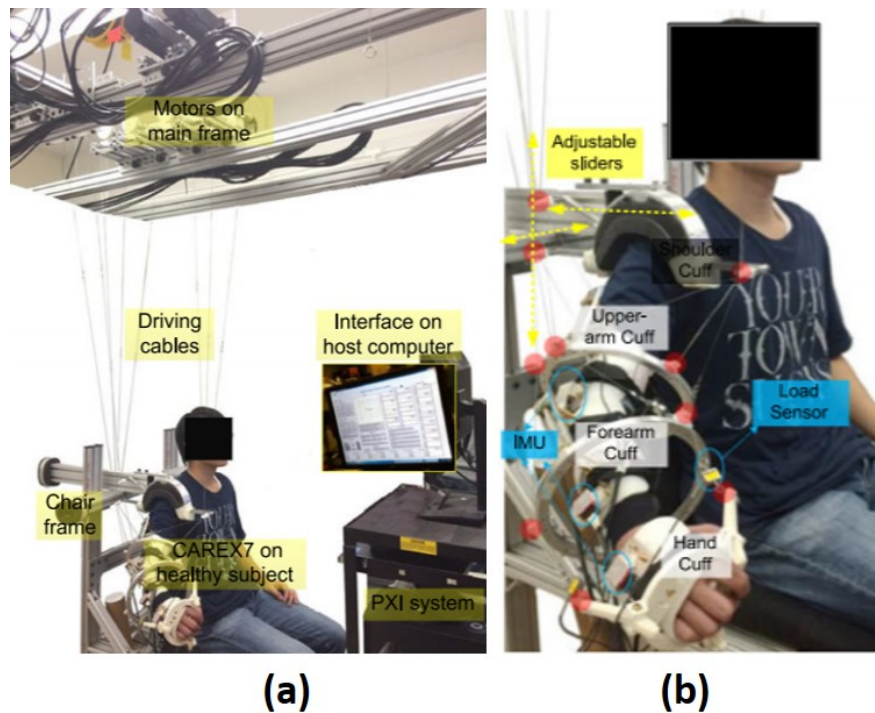
Figure 1.1. A (a) subject shown with the CAREX-7 robot system and (b) a subject wearing the CAREX-7 arm attachment as seen in the work by Cui et al. [1].
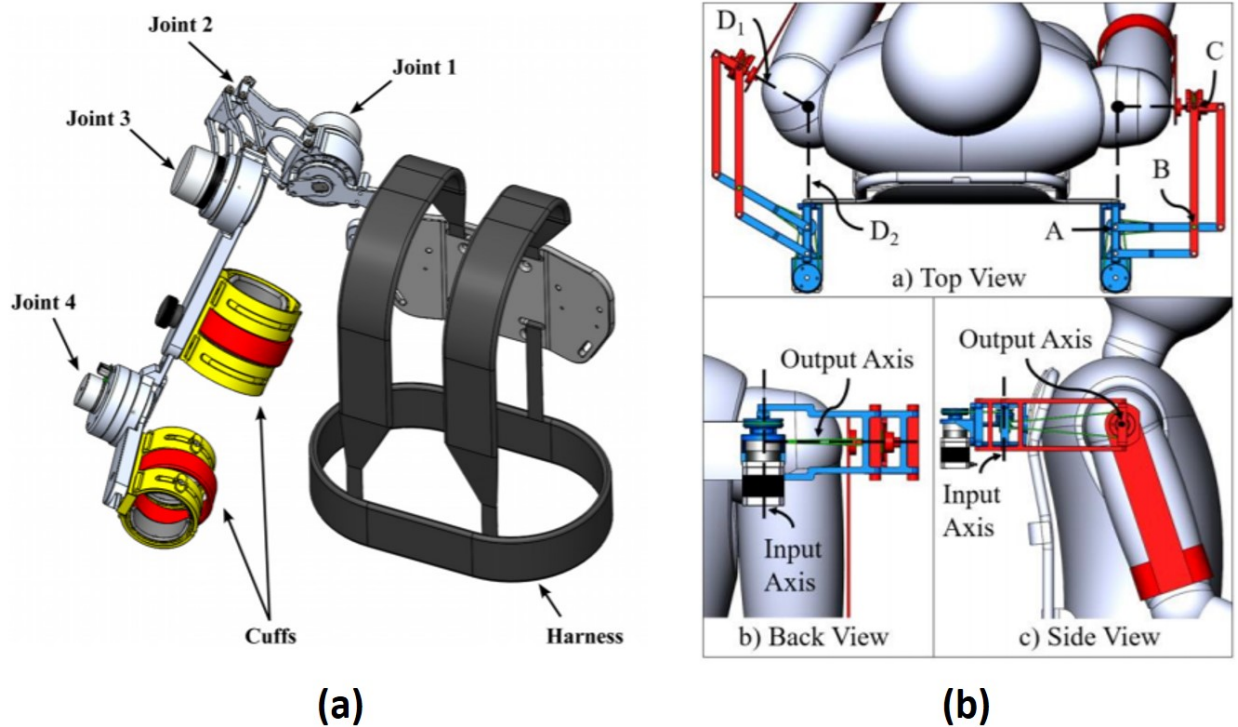
Figure 1.2. The (a) proximally located actuator design by Christensen et al. [2] and (b) the distally located actuator design by Jones et al. [3].

the DPL prevents any restrictions in shoulder movement. Jones et al. [3] also used the DPL system to mimic the work-space of a shoulder, but utilized a pulley system to distally locate the motor on the back of the wearer. This design can be seen in figure 1.2b. By distally locating the motor, the weight of the motor is not on the arm which could further improve arm mobility while wearing the device.

Since these exoskeletons will be worn by the user, the ergonomics of the exoskeleton are important to limit discomforts or prevent injuries to the wearer. A main ergonomic characteristic of exoskeletons are their weight. In several studies on loads placed on the back while walking, it was discovered that the load should not exceed 10% of the wearer's body weight [35, 36, 37]. It was also noted by Chen et al.[36] that subjects experienced the least amount of discomfort when the load was located near the T12 vertebrae.

4

1.3 Anatomical Terminology

Throughout this thesis, anatomical terminology will be used to describe various planes and directions with respect to the human body. When describing human motion, an anatomical plane is often referenced. Figure 1.3a shows the three anatomical planes. The first plane of reference is the frontal plane. This plane divides a person into two sections parallel with the stomach and the back. The second plane of reference is the transverse plane which divides a person into two sections at the torso. The last anatomical plane is the sagittal plane. This plane divides a person into left and right halves. In addition to referencing the anatomical planes, position terms will be used to describe the location of an object with respect to an anatomical point. The two main terms used are if an object is
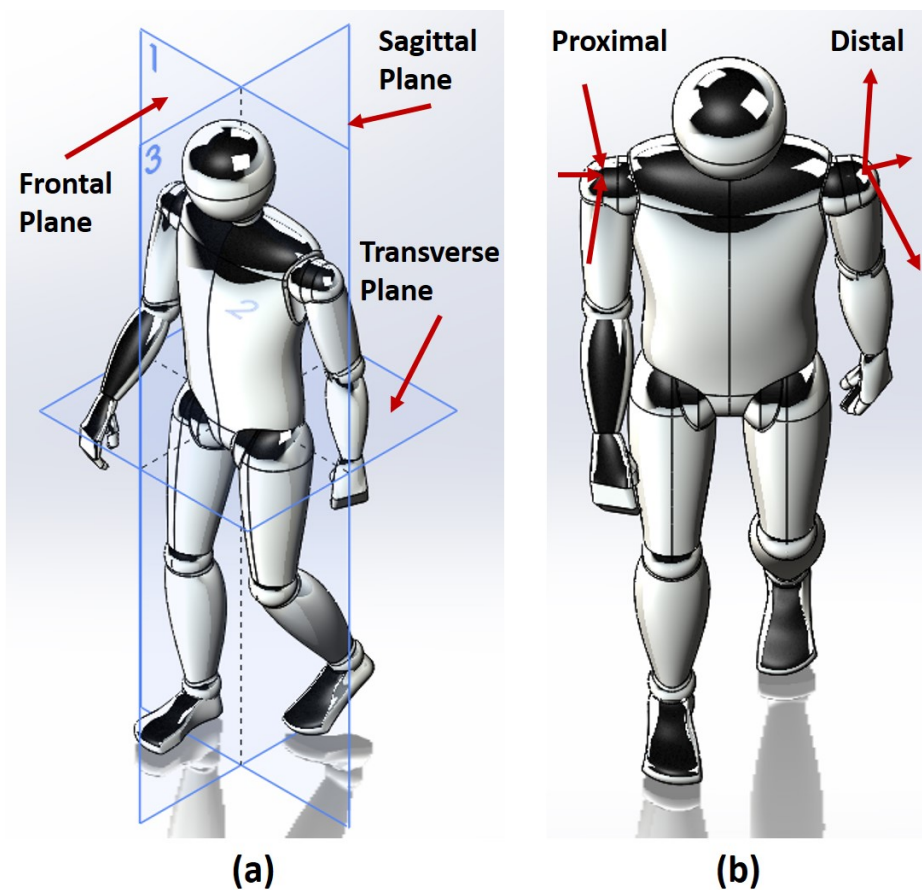
Figure 1.3. The (a) three anatomical planes and (b) defining how something can be distally and proximally located with respect to the shoulder.

distally or proximally located with respect to a point. Figure 1.3b shows an example for each with respect to a shoulder. Distal refers to an object being located away from the shoulder, while proximal refers to the opposite. Throughout this thesis these planes and terms will be used to describe biomechanical changes in gait and design characteristics of exoskeletons.

In addition, understanding how the shoulder moves is also important. Figure 1.4 shows the anatomy of the shoulder and movements the shoulder can perform. The shoulder is made up of two main components called the glenohumeral joint and the shoulder girdle. The shoulder girdle is comprised of the sternoclavicular joint, the acromioclavicular joint, and the scapulothoracic joint which can be seen in figure 1.4a. The glenohumeral joint is often referred to as the "shoulder joint" since it solely contributes to abduction/adduction, flexion/extension, and internal/external rotation when the elevation of the arm is less than 90° [2]. However, when the elevation of the arm is above 90°, the shoulder girdle contributes to these movements. When this occurs the center of rotation of the shoulder can shift from the center of the glenohumeral joint. This shift in center of rotation should be accounted for to reduce misalignments when designing an upper extremity exoskeleton.
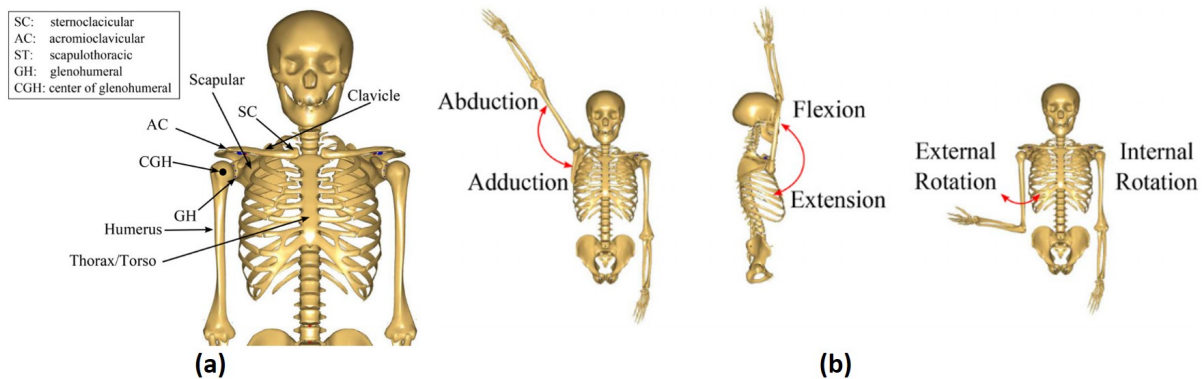
Figure 1.4. The shoulder (a) anatomy and (b) movements as originally presented by Christensen et al. [2].

1.4 Goal of Thesis

The purpose of this thesis is to aid in the investigation of utilizing arm swing for gait rehabilitation. Two tasks were performed in this thesis. The first task was a study on how forearm movements effect gait. This was done by observing full body kinematics, spatiotemporal parameters, muscle activity, interlimb coordination, and metabolic energy expenditure. This study gives insight on how the forearm is controlled during walking, but also how better to design and control a forearm prostheses. The second task performed was the introduction of a novel distally located upper extremity exoskeleton to assist with arm swing. Figure 1.5 shows a model of the exoskeleton on both arms of a person. This
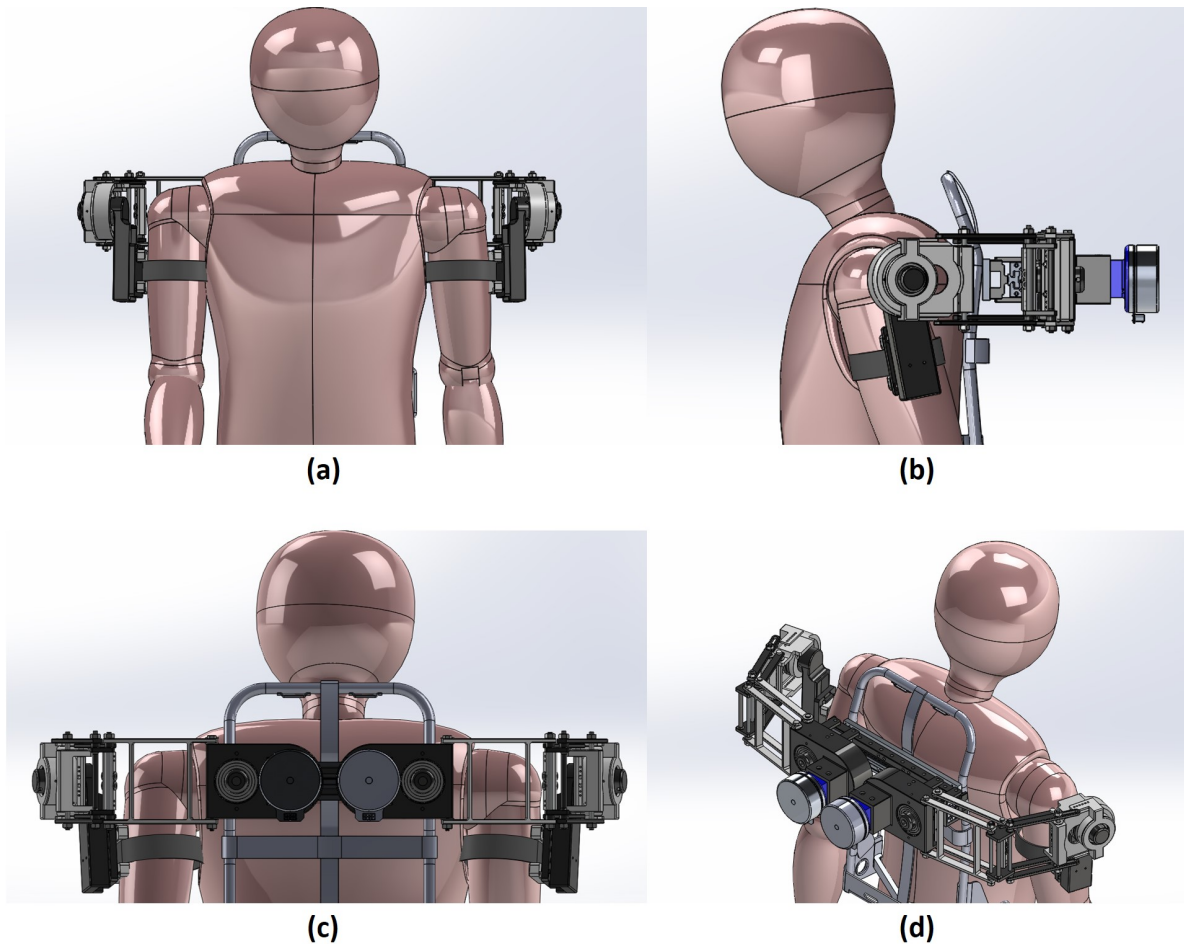
Figure 1.5. A (a) front view, (b) side view, (c) back view, and (d) isometric view of a person wearing the exoskeleton on both arms.

exoskeleton utilizes a hybrid DPL, weighs less than 10% of the average adult, and only a fraction of the weight is felt on the wearer's arm. The goal of this thesis is to provide more insight into arm swing mechanics and methods for arm swing rehabilitation.

CHAPTER 2

THE EFFECTS OF FOREARM MOVEMENT ON HUMAN GAIT AT DIFFERENT SPEEDS

2.1 Methods

2.1.1 Subjects

Twelve young adults with healthy gaits participated in the study. Half were male and the other half were female to mitigate the effects of gender. The age range for our subjects was from 21-27 years (22.3 ± 1.83 years) reported as (mean $\pm$ standard deviation). The subjects' body masses ranged from 54.4-82.1 kg (63.8 ± 8.6 kg) and heights ranged from 1.55-1.90 m (1.70 ± 0.10 m). This population was desired since all of the subjects had healthy gaits which allowed us to directly compare testing conditions. The subjects determined their self-selected normal and fast speeds and were later asked to walk at these speeds. These walking speeds ranged from 0.67-1.25 m/s (0.92 ± 0.2 m/s) for the normal speed, and 1.11-1.78 m/s (1.36 ± 0.2 m/s) for their fast selected speed. This study was approved by the Institutional Review Board of the University of Maine.

2.1.2 Experimental Procedure for EMG and Motion Capture

First, subjects were asked to walk on a treadmill (TT8, Sole, USA) and determine their "normal" and "fast" walking speed. Next, electromyography (EMG) sensors (SP-W02-0037, Delsys, MA, USA) were placed on key upper extremity muscles used for arm swing. These muscles are muscles outlined by Kuhtz-Buschbeck et al. [23] with the addition of the external obliques. The muscles observed included the bicep brachii (BB), tricep brachii (TB), pectoralis major (PM), external obliques (EO), trapezius (TP), latissimus dorsi (LD), anterior deltoid (AD), and posterior deltoid (PD). EMGs were placed on both the left and right side. Figure 2.1 shows the muscles targeted.

9
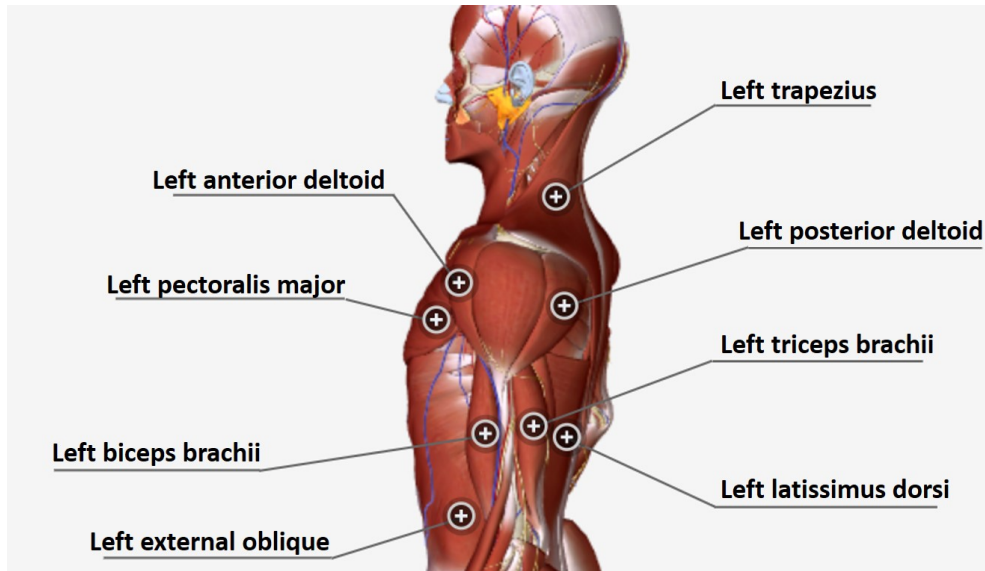
Figure 2.1. Upper extremity muscles observed (BioDigital Inc.).

Table 2.1. Exercises to elicit MVCs for normalizing the EMG signals.

Muscle	MVC Exercise
Biceps Brachii	Flexion of elbow from rest to maximum point
Triceps Brachii	Extension of elbow from rest to maximum point
Pectoralis Major	Press palms together anterior to sternum along the sagittal plane
Trapezius	Abduction of arms 45° between frontal and sagittal planes
Latissimus Dorsi	Movement of the elbow from anterior to postior along the trunk
Anterior Deltoids	Overhead shoulder press while keeping the elbow parallel to the sagittal plane
Posterior Deltoids	Seated bent over dumbbell raise without weight
External Obliques	Trunk and arm rotation with hands interlocked

Next subjects were asked to perform maximum voluntary contractions (MVCs). MVCs are required in order to compare different people due to varying levels of fitness. Table 2.1 outlines the MVCs for each muscle. The MVC isolates the muscle so that the maximum muscle activity for that muscle is known. These MVCs were used to normalize the EMG data for each person so that the EMG activity between people could be directly compared. These MVCs were collected using Nexus software (Vicon, UK).

Once the MVCs were collected, motion capture markers were placed on the subject. A nine camera Vicon motion capture system was used to track the markers' trajectory to collect all kinematic data. Kinematic and EMG data was captured simultaneously. Figure 2.2a,b shows the markers on a subject and the placement of each of the markers on the

Figure 2.2. A (a) subject wearing markers, (b) marker placements, and (c) the Nexus motion capture software.

subject. Figure 2.2c shows the Nexus software tracking marker trajectories as a subject walked.

After the markers were placed on the subject, the subjects then walked under three different conditions at both their normal and fast walking speeds. Figure 2.3 shows a subject walking in all three conditions. The first condition was the natural walking condition (NW). Subjects walked normally with no change to their forearm motion. The second condition, the artificial forearm condition (AW), involved attaching an arm brace with a 3D printed passive artificial forearm to the subject and restricting their forearms at 90°. This artificial forearm is meant to replace their actual forearm while walking. The artificial forearm was designed to replicate an actual forearm and weighs 1.25 kg which is in the range of estimated male and female forearm masses [38]. In addition, the elbow joint of the artificial forearm was restricted to avoid hyperextension of the elbow joint. The use of a slider joint was used to ensure that the passive elbow joint was parallel to the subjects elbow. The artificial forearm can be seen in figure 2.3d. The third condition was the restrained walking condition (RW). This condition consisted of only restraining the forearms at 90° similar to the previous condition. The forearms were constrained the same

11

Figure 2.3. A subject performing (a) natural walking, (b) walking with the artificial forearms, (c) walking with their arms restrained, and (d) the artificial forearm and the elbow brace.

way to account for how they had to be constrained with the artificial forearm. The speeds and conditions were fully randomized during the experiments.

2.1.3 EMG and Motion Capture Data Processing

Joint angles were calculated for the shoulder, trunk, hip, knee, and ankle. In addition, stride length and cadence were also calculated. Joint angle calculations were performed using Visual 3D (C-Motion, MD, USA) by assigning a skeleton model to the marker trajectories previously captured. Figure 2.4 shows how the marker trajectories were labeled and how a skeleton model was assigned to the markers. From Visual 3D, the data was exported to MATLAB (Mathworks Inc.) for further analysis. To filter the joint angles, a second-order zero-lag Butterworth filter was utilized with a cutoff frequency of $6\,\mathrm{Hz}$. Similarly, the EMG signals were filtered using a second-order zero-lag Butterworth filter with a cutoff frequency of $50\,\mathrm{Hz}$. The EMG signal then underwent a root means square wave rectification.
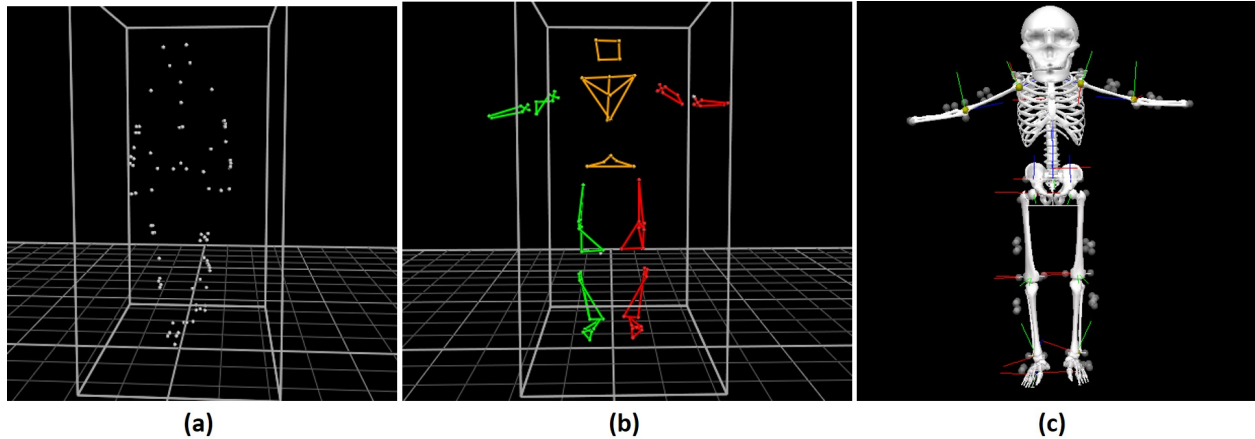
Figure 2.4. The (a) marker trajectories, (b) labeling model in Nexus, and (c) the skeleton model applied in Visual 3D.

2.1.4 Metabolic Expenditure Measurements

Five of the subjects (21.8 ± 0.45 years, 65.2 ± 9.15 kg, 1.76 ± 0.09 m, 0.96 ± 0.21 m/s, 1.38 ± 0.19 m/s) performed metabolic expenditure measurements. A metabolic breath analyzer (PNOE, CA, USA) collected and computed data such as the amount carbon dioxide exhaled (VCO_2) and expended energy. Figure 2.5 shows a subject walking while wearing the metabolic breath analyzer. The subjects performed the same conditions as outlined above. However, subjects were asked to walk for five minutes during each condition to reach steady state breathing. Only the last minute of walking was analyzed. This reduces any spikes in CO_2. Between conditions and speeds, five minutes of rest was implemented to allow the subject to fully recover. After the experiment, data was exported from the client portal to MATLAB.

2.1.5 Data Analysis

Kinematic and EMG data were segmented based on the subject's gait cycle. This was done by utilizing the ipsilateral foot's heel strikes to determine a gait cycle. At least ten gait cycles were used for each joint and muscle. Figure 2.6 shows an example of how a joint was segmented. Once segmented, the left and right sides' trajectories were combined

13
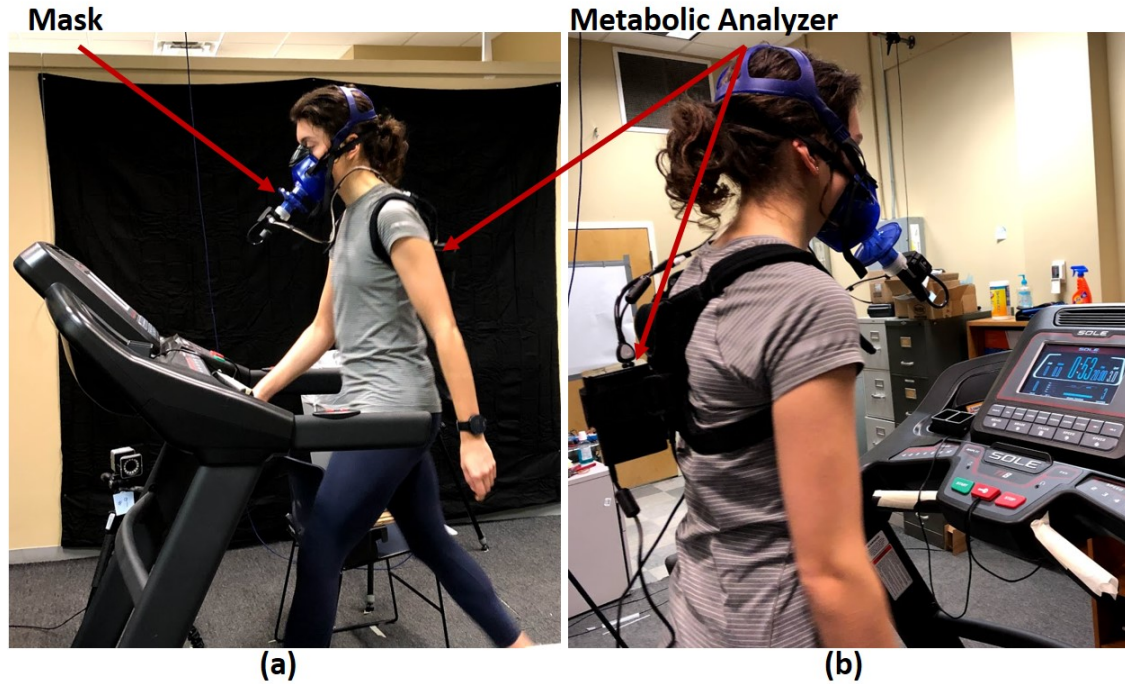
Figure 2.5. A (a) side and (b) back view of a subject wearing the PNOE metabolic analyzer.
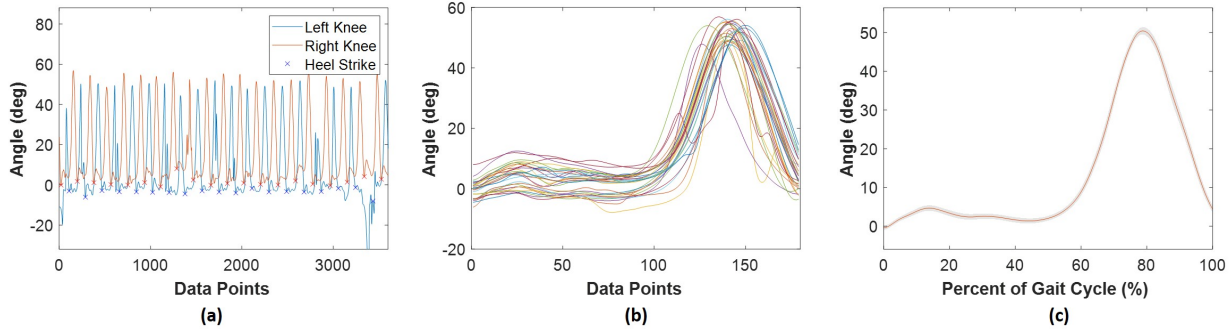
Figure 2.6. The segmentation of a knee joint angle from (a) the entire condition, (b) segmented by heel strikes and combined, and (c) the mean joint angle with standard error.

except for trunk twist. The segmented data for an example knee can be seen in figure 2.6b. The trunk twist remained two separate variables where the right trunk twist was segmented using right heel strikes and the left trunk twist was segmented using left heel strikes. The range of motion (ROM) of the joints were then calculated by subtracting the maximum angle by the minimum angle during a gait cycle. This was done to compare joint

14

movement between conditions. All of the joint angles rotated in the sagittal plane except for trunk twist, which occurred in the transverse plane.

Spatiotemporal values such as stride length and cadence were also calculated. These were calculated using the paved length during a gait cycle and the number of cycles per minute. The interlimb coordination was quantified by using the point estimates of relative phase (PERP) between the contralateral hip and shoulder angles [12, 16]. To determine the magnitude of any changes in coordination the absolute values were determined. One-way ANOVA statistical analysis with two-tailed $\alpha = 0.05$ was used to determine statistical significance between experimental conditions.

After the EMG signals were segmented, they were normalized based on their MVCs. This method was previously outlined by Kuhtz-Buschbeck et al. [23]. The overall mean was then calculated for each muscle similar to what was done by Canton et al. [22]. Next, the mean EMG values of the AW and RW conditions were normalized based on the values from the NW condition. They were then presented as a percent for both the "normal" and "fast" speeds. This allowed for the comparison of muscle activity over the entire gait cycle.

2.2 Results and Discussion

2.2.1 Kinematic and Spatiotemporal Parameters

The ROM of the joint angles as well as stride length and cadence can be seen in figure 2.7. Figure 2.7 shows that the shoulder angle ROM significantly decreased in the AW and RW conditions at the "normal" speed when compared to the NW condition. In addition, it shows that shoulder angle decreases significantly at the "fast" speed for the AW condition when compared to the other two conditions. This can be seen for the trunk twists as well. During the AW condition, the range of motion for both the left and right trunk twist significantly decreased at both speeds. There was no statistical difference between the NW and RW for these joints. Restraining the forearms seemed to have no significant effect on trunk twist. Angelini et al. [39] also noticed a minimal change in trunk twist when

15
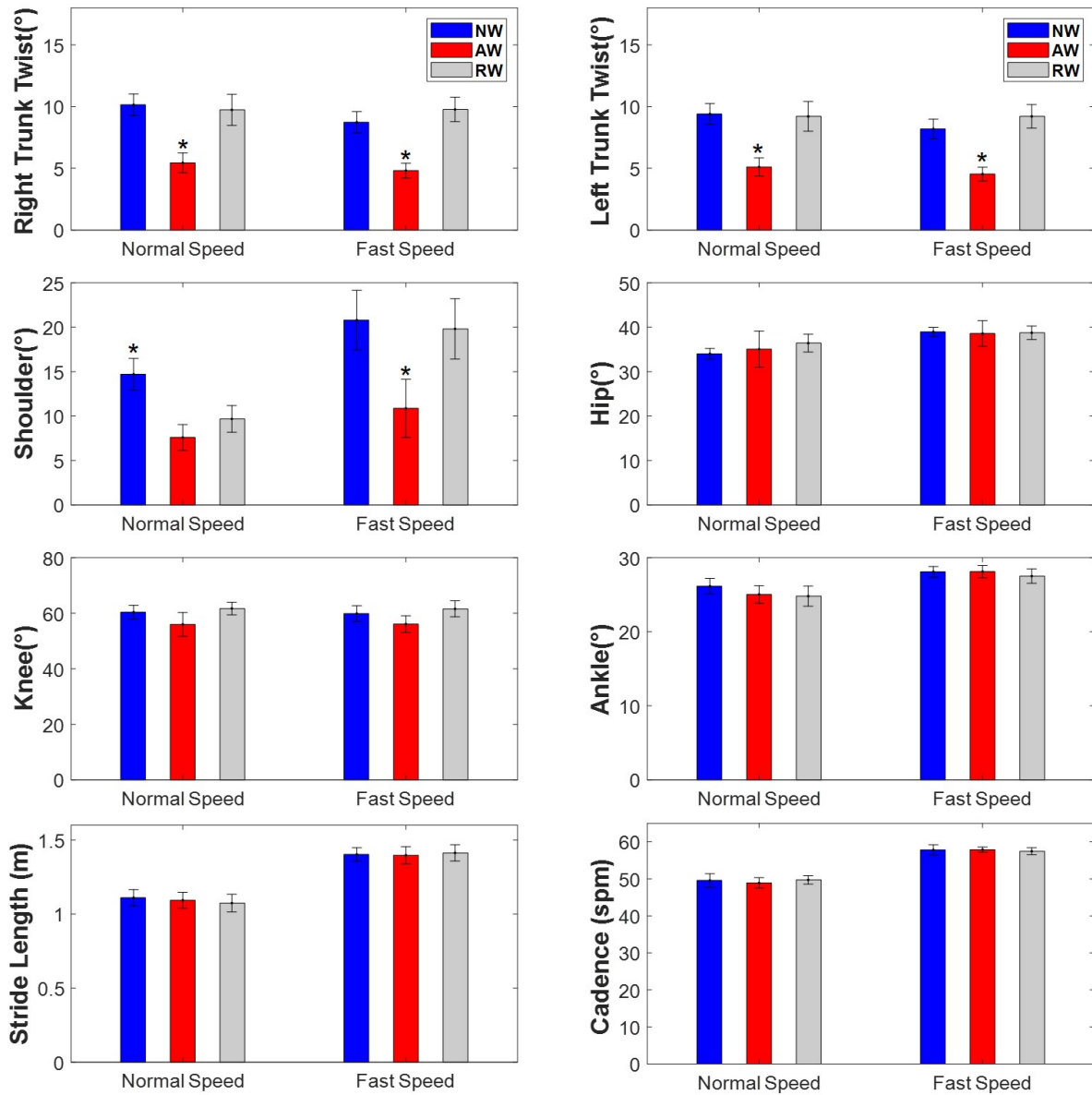
Figure 2.7. The ranges of motion for the key joint along with stride length and cadence (mean±standard error). An asterisk (∗) indicates a significant condition.

restraining the forearms when they observed no changes in thorax rotation due to the changes in the arm swing. Overall, it can be noted that the artificial forearm only effected upper extremities. Since the forearms were restrained in the RW condition, it can also be

16

concluded that the changes observed in the AW condition were not caused by restricting the forearms.

Despite changes in upper extremities, the lower extremities remained unaffected throughout the experiment. It can be seen in figure 2.7 that there are no significant changes in joint angles, as well as no changes in stride length or cadence. These findings are supported by Wu et al. and Pontzer et al. [11, 20] who observed that lower extremities could remain unaffected by changes to the upper extremities. The changes in the upper extremities when wearing the artificial forearm are likely an attempt to control any unwanted movements. These unwanted movements were not present in the RW condition, and that condition remain most similar to the NW condition. As expected, the NW and RW condition remained similar since restraining the forearms is often a way the body actively controls forearm motion at faster speeds.

Table 2.2 shows the PERP values for each condition. It can be seen that the PERP values increased during the AW condition with a significant increase at faster speeds. Although there was not a significant difference at normal speeds, there was still a large increase during the AW condition, but with high variability (standard error). PERP values show the out-of-phase motion between the hip and shoulder joints which helps identify uncoordinated movements between limbs. This shows that the addition of an artificial forearm increases uncoordinated movements and instability.

The relationship between trunk twist and the shoulder joint was further investigated using the cross-correlation between their trajectories. Table 2.3 shows the maximum cross-correlation coefficients and subsequent time lags. The opposite signs indicate that the

Table 2.2. The PERP values reported as mean±standard error. An ($*$) indicates a condition significantly different from others.

Condition	Normal Speed	Fast Speed
NW	32.19° (±4.72°)	17.04° (±1.71°)
AW	54.03° (±12.05°)	60.39° (±13.81°)*
RW	43.15° (±5.62°)	22.96° (±2.86°)

Table 2.3. Shoulder-trunk cross-correlations for the tested conditions.

Correlation Coefficient	Shoulder-Right Trunk		Shoulder-Left Trunk	
	Normal	Fast	Normal	Fast
r_{NW}	0.98	0.96	-0.97	-0.95
r_{AW}	0.82	0.85	-0.81	-0.84
r_{RW}	0.94	0.97	-0.94	-0.96

left and right trunk twist move in opposite directions when compared to the shoulder joint. The high correlation coefficients indicate that the maximum angle of rotations occurred at almost the same time. The NW condition reported very high correlation coefficients with the RW condition reporting slightly lower values. However, it can be seen that at both speeds there is a decrease in correlation for the AW condition. This indicates that there is a time gap between the maximum angle of rotation of the trunk and shoulder joint. This further suggests that the artificial forearm caused uncoordinated movements between joints and possibly caused these joints to work separately to mitigate any unwanted movements.

2.2.2 EMG Signals

Figure 2.8 shows the muscles with increased changes in muscle activity. Similar to the joint angles, the EMG signals are shown with the left and right sides combined and displayed as a percent of a gait cycle. The mean muscle activity across the gait cycle were computed. In order to compare muscle activities, the NW condition was used as a baseline and used to normalize the AW and RW conditions. Table 2.4 show EMG signals of the AW and RW conditions normalized by the NW condition. It can be seen in figure 2.8 that there was an increase in muscle activity in the biceps, triceps, trapezius, and the anterior and posterior deltiods. The largest increases in muscle activity occurred during the AW condition. Significant increases in muscle activity occurred in the biceps (BB) at both speeds as well as in the trapezius (TP) at normal walking speed. This can be seen in table 2.4. The biceps are used to control forearm movements as well as provide dynamic stability for the front of the shoulder at the beginning and end of a gait cycle. The increase in

Table 2.4. EMG signals when normalized by the NW condition reported as mean±standard error. An (∗) indicates the AW and RW conditions are significantly different, whereas a (+) indicates a significant change in the mean EMG when compared to the NW condition.

Condition	BB (%)	TB (%)	PM (%)	EO (%)	LD (%)	TP (%)	AD (%)	PD (%)
Normal Speed								
AW	60.33 (±22.62)*+	2.56 (±1.64)	1.96 (±2.19)	2.41 (±1.94)	0.37 (±1.86)	47.23 (±19.61)*+	12.00 (±14.07)	38.60 (±17.75)
RW	32.90 (±20.10)	16.13 (±15.06)	1.26 (±2.22)	0.44 (±0.73)	0.48 (±1.05)	22.66 (±11.20)	3.74 (±10.71)	14.01 (±10.29)
Fast Speed								
AW	71.01 (±24.41)*+	8.12 (±4.84)	2.68 (±2.10)	0.53 (±1.77)	0.14 (±2.85)	43.35 (±17.46)	27.55 (±16.34)	26.84 (±17.56)
RW	35.18 (±22.28)	31.34 (±27.74)	0.99 (±2.00)	0.65 (±2.07)	0.33 (±1.71)	27.82 (±7.25)	16.81 (±10.74)	13.60 (±8.87)

muscle activity in the biceps during the AW condition is due to the biceps attempting to provide more stability to the shoulder. It can be seen in figure 2.8 that the EMG signal for the biceps not only increases at around 60%, but also increases at the beginning and end of the gait cycle. It should also be noted that for this condition the shoulder ROM decreased. The increase in muscle activity suggests that the increase was used to reduce arm swing and unwanted movements of the artificial forearm.

Similarly, the trapezius increased for both speeds during the AW condition. The trapezius muscle is used to stabilize the shoulder blade to enable the shoulder joint to rotate. The peak muscle activity in the trapezius occurred around the same time as the maximum flexion of the shoulder during the AW condition. Similar to the bicep, this indicates that the contraction of the muscle was used to reduce arm swing in an attempt to reduce uncoordianted movements. This behavior was also observed by Kuhtz-Buschbeck et al. [23] when they asked subjects to hold their arms parallel to their trunk. These findings further support the idea that muscle activity increased while wearing the artificial forearm to better control its movements.

Small increases in muscle activity were also noticed in the anterior (AD) and posterior deltiods (PD). The purpose of the anterior deltiod is to flex the shoulder while the posterior deltiod extends the shoulder. When observing the AD, there was a peak in muscle activity at around 20% and 90% of the gait cycle in the NW and RW conditions at the fast speed. This is due to the the AD muscle generating flexion for the shoulder. However, these peaks are not seen in the AW condition for this muscle. Instead there is a peak at around 50% of
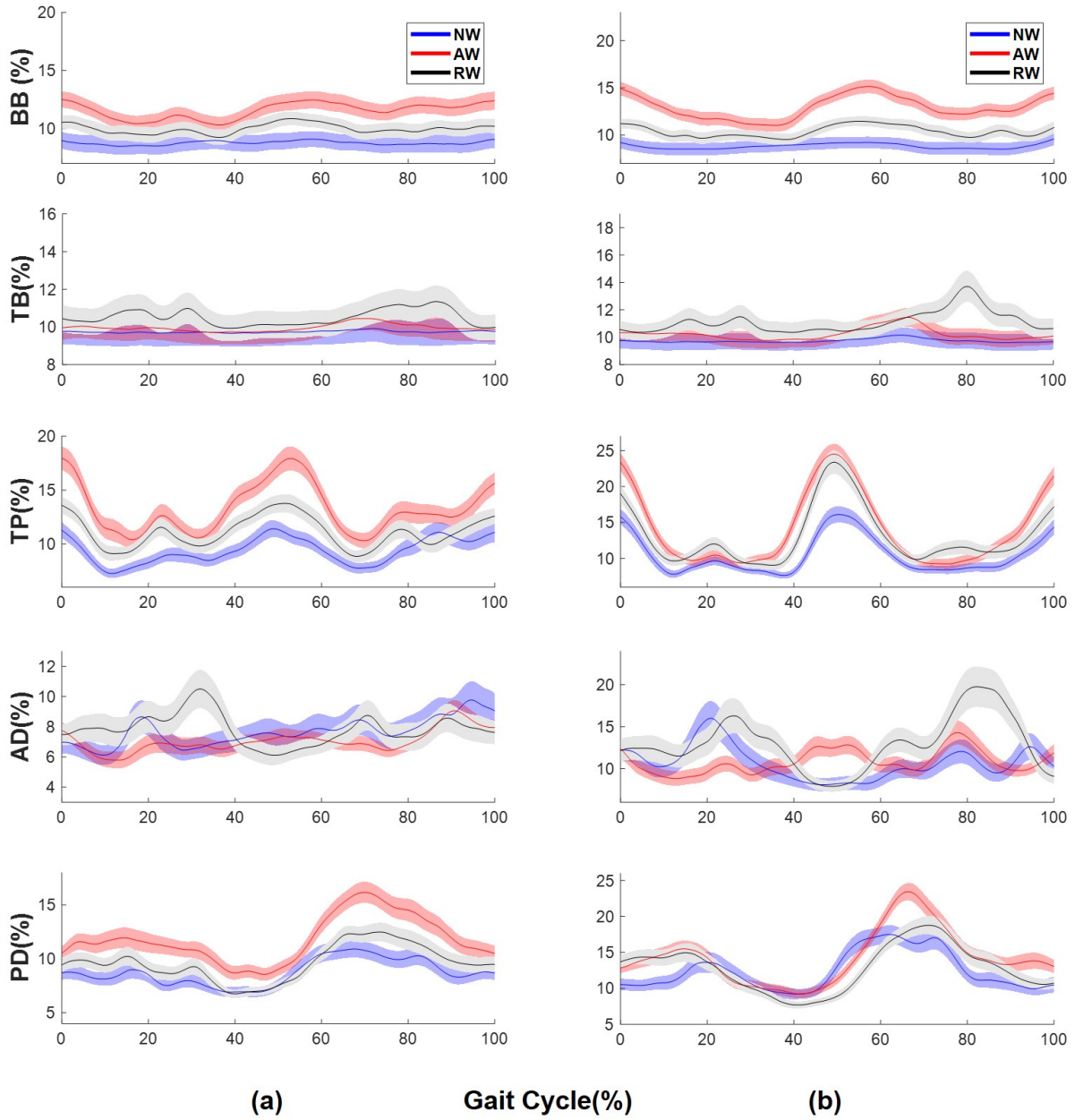
Figure 2.8. EMG signal normalized with MVCs for all three conditions at the (a) normal and (b) fast speeds (mean±standard error).

the gait cycle (shoulder maximum flexion) indicating that the ADs were used more to stabilize shoulder movement than generate flexion when wearing the artificial forearm.

It can be concluded that the increase in muscle activity observed is a result of the body actively trying to stabilize the restricted forearms and artificial forearms. This is supported by the reduced ROM in the shoulder and trunk mentioned earlier. In addition, it is also supported by findings from Kuhtz-Buschbeck et al. [23] who noticed that muscles will activate even when restrained to stabilize a limb. A feedback control system can be used to parallel the bodies' response to the various conditions. The muscle activity acts as a control input to the system, which in this case is the body. When walking normally, there is minimal muscle activity due to the body achieving its optimal gait parameters such as ROM and interlimb coordination. However when an external disturbance is present such as the artificial forearms, the upper extremity control system attempts to mitigate unwanted movements through the use of increasing muscle activity mainly in the biceps, triceps, trapezius, and anterior and posterior deltiods. These muscles contract eccentrically to reduce rotation in the shoulder and trunk. These changes were present at both speeds in the AW condition indicating that there is an active control system for controlling forearm motion during walking. Due to the reduced cross-correlation in movements between the shoulder and trunk joint there may be two control systems used to mitigate the undesired effects in the AW condition. When only restraining the forearms, the control system responded most similar to that of just naturally walking.

2.2.3 Metabolic Expenditure

Figure 2.9 shows the metabolic changes during each condition. The energy expended during each condition is shown in figure 2.9a while the normalized increase in expended energy is seen in figure 2.9b. The energy increase for the AW and RW conditions were normalized using the NW values. It can be seen that at lower speed there is no difference between conditions, however at the faster speed there is an increase in the energy expended

21
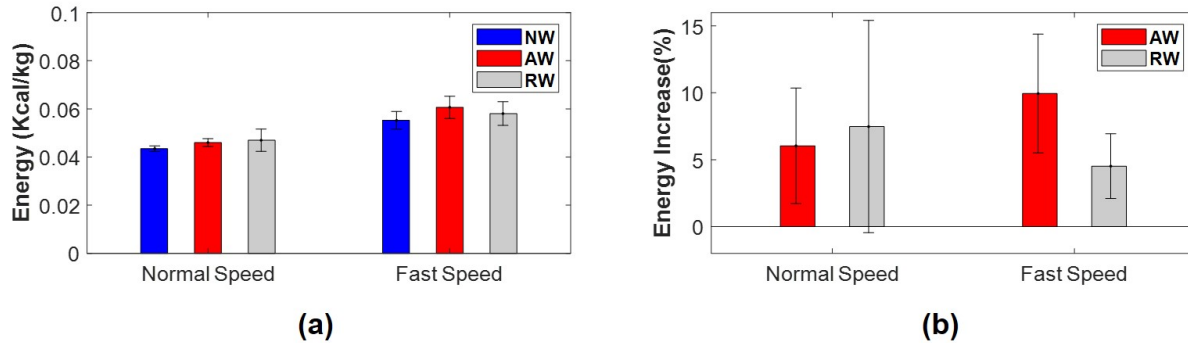
Figure 2.9. The (a) net energy expenditure normalized by the weight in each condition and (b) the amount of energy increase compared to natural walking.

during the AW condition which is approaching statistical difference ($p = 0.069$). For the AW condition at a fast speed, the energy consumption increases 9.94%. These results are in line with Umberger [40] who observed an increase of 5% when restricting the forearms during walking. This also supports the findings that arm swing helps reduce energy expended during walking [4]. The shoulder joint ROM was reduced when wearing the artificial forearms, as seen in figure 2.7, which may account for the increase in energy expended during this condition. These results are also supported by Yegian et al. [24] who observed an increase of 11% in oxygen consumption when the forearms were constrained.

2.3 Conclusion

In this study, the effects of forearm movements on walking gait were observed. The goal was to determine if the forearm is actively or passively controlled by the body. Twelve subjects walking at self selected speeds under three conditions. The first condition involved walking normally, the second condition involved wearing a 3D printed passive artificial forearm with the forearms restricted to 90°, and the third condition just had the forearms restrained at 90°. The artificial forearm was designed to mimic an elbow, forearm, and hand. It was discovered that the addition of the artificial forearm caused changes to the

upper extremities kinematics, EMG signals, and energy expended. The ROM of the shoulder and trunk joints both decreased when wearing the artificial forearm, while the muscle activity increased in the biceps, trapezius, and a partial increase in the deltiods. Energy consumption also increased around 10% at faster speeds. No change in lower extremity kinematics or spatiotemporal parameters were observed.

The addition of the artificial forearm decreased the coordination between limbs resulting in instability. This was especially true at faster speeds. When only the forearms were restricted in the RW condition, gait parameters and muscle activity was most similar to the NW condition. The changes observed in the AW condition serve to mitigate unwanted movements caused by the passive artificial forearm. The body uses an increase in muscle activity to cause a decrease in joint rotation. However, this increase in muscle activity would also cause an increase in energy consumed. This study can be used to help better design and control forearm prostheses. Based on these results, a forearm prosthetic requires an active control system while walking to help maintain interlimb coordination and natural walking mechanics.

CHAPTER 3

A DISTALLY LOCATED UPPER EXTREMITY EXOSKELETON FOR GAIT REHABILITATION

3.1 Exploring the Design Space

The main design goals of this exoskeleton were to mimic the work-space of a healthy shoulder while being ergonomically friendly to the wearer. When exploring the design space, initially the ability to mimic a healthy shoulder's work-space was investigated. Designs were evaluated on their ability to mimic the work-space of the shoulder, transfer torque to the arm, and on the design's ergonomic characteristics. Figure 3.1a shows the first conceptual design to achieve this work-space. This design consisted of a watchband linkage system that could arc from a backpack to a shoulder. The idea was that these linkages would act similar to how a watchband wraps around a wrist, providing flexible movement for the internal and external rotation of the shoulder. However, due to the number of degrees of freedom, singularities would occur in the work-space and cause the linkages to become stuck. The next design was based on the work of Bouffard [41] and Jones et al. [3]. This design is seen in figure 3.1b. It utilized a hybrid DPL and a distally located actuator. Torque was transferred from the motor to the end effector through a pulley system. This
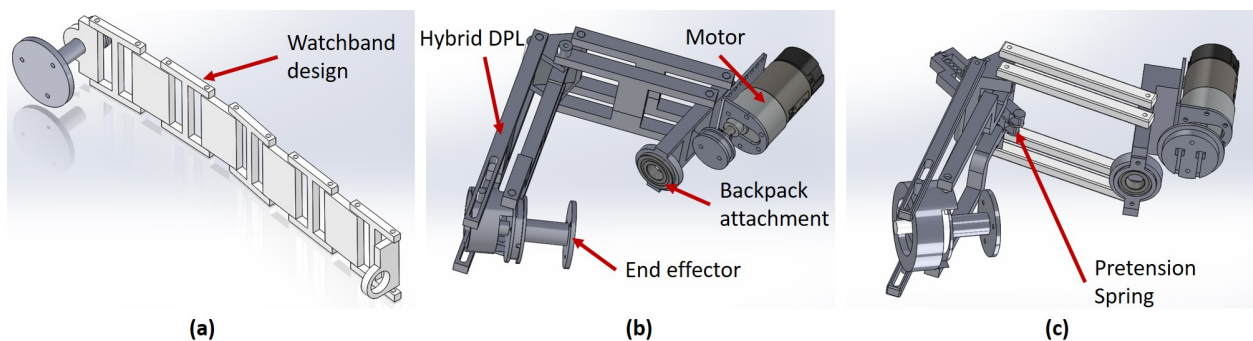
Figure 3.1. The (a) watchband design, (b) distally located design, and (c) the distally located design with a pretensioning device.

design only used a small motor and acted as a proof of concept design. However, this design suffered from significant slack in the pulley system which significantly reduced its ability to transfer any torque. To try and compensate for this slack a pretensioning spring was placed along the pulley's path. The design can be seen in figure 3.1c. The addition of the pretensioning system helped only slightly to reduce slack in the pulley.

In addition to investigating distally located actuator designs, a proximally located actuator design was constructed as seen in figure 3.2. This design utilizes the hybrid DPL to mimic the work-space and it is also the first attempt to design a way to attach the exoskeleton to the subject. However, due to the motor being located on the arm, it was determined that this could restrict motion and was not ergonomically friendly for the wearer. Methods to counter balance the motor were investigated, but it was found a counter weight would add unnecessary weight to the system. It was then determined that the best design would be to use either a DPL or hybrid DPL mechanism to mimic the
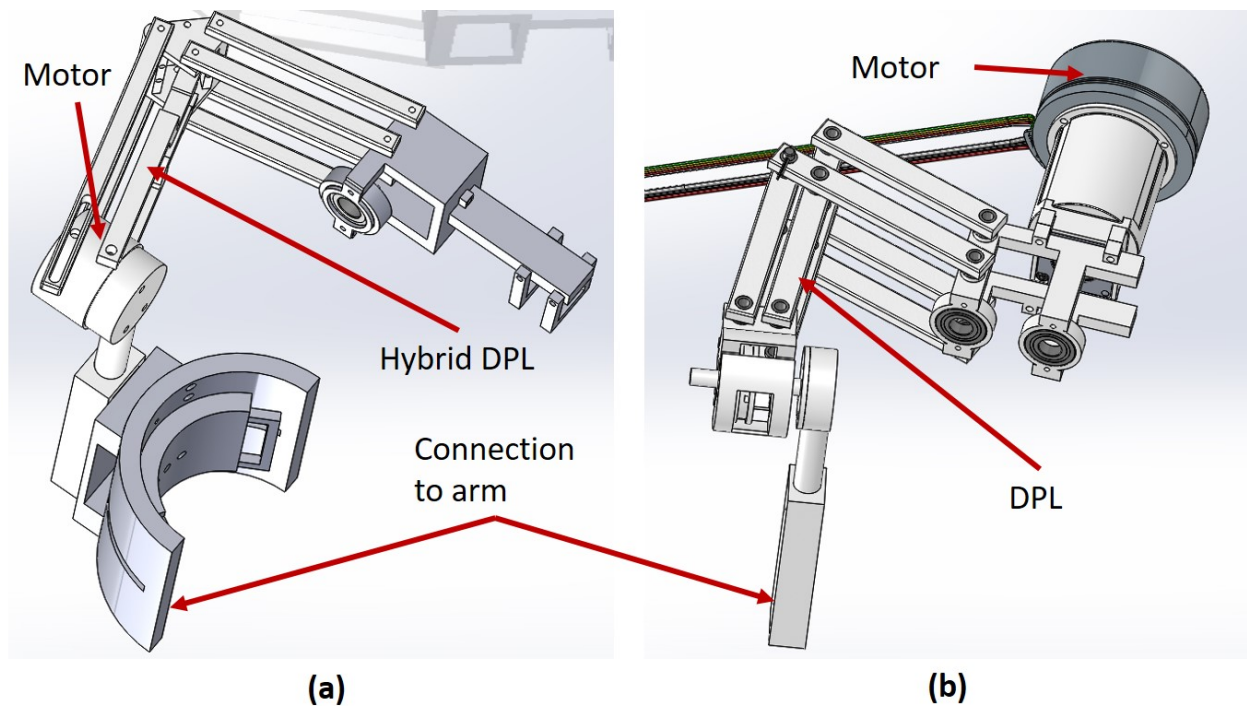
Figure 3.2. A (a) proximally located motor design and (b) a distally located design with a traditional DPL.

work-space of the shoulder and that the motor should be distally located. Figure 3.2b shows a distally located motor with a DPL.

Based on the design of Jones et al [3], a mature version of the design he proposed was created. This can be seen in figure 3.3. The motor acts as a counterweight in this design and offsets some of the weight off of the arm. The exoskeleton attaches to the wearer via an arm brace. In addition, this design utilizes constraint points along the DPL to direct the pulley system. It was discovered while designing this system, the slack issue experienced in earlier designs was caused by insufficient constraint points along the DPL. Due to the characteristics of the DPL, the work-space of the exoskeleton was limited to a fixed radius of rotation. However, it is known that the shoulder's center of rotation can shift as the arm moves. This is not ideal if multiple people of varying body types want to wear the exoskeleton. The fixed radius restricts the exoskeleton's ability to accommodate different shoulder sizes.

To provide a larger work-space a hybrid DPL was introduced to the system, similar to the design seen in figure 3.1b. Now that the slacking issue in the pulley system has been improved, this design is a viable option. Figure 3.4 shows the final design for the

(a) (b) (c)
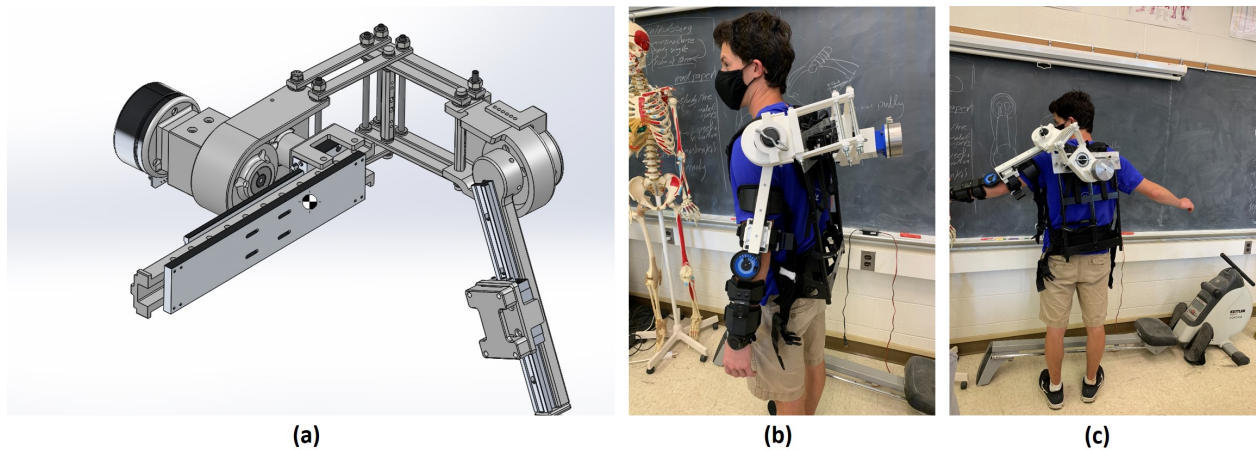
Figure 3.3. A (a) front view of the exoskeleton with a traditional DPL, (b) a side view of a subject wearing the exoskeleton, and (c) the subject performing a T-pose with the exoskeleton.
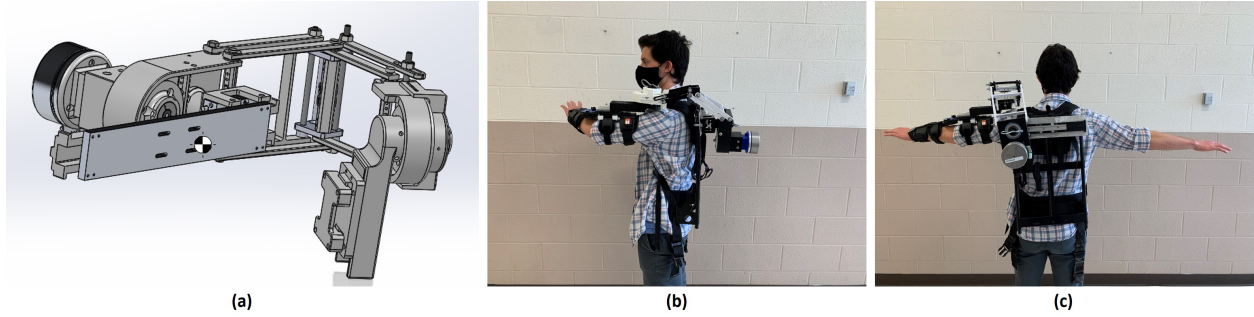
Figure 3.4. A (a) front view of the exoskeleton with a hybrid DPL, (b) a side view of a subject wearing the exoskeleton, and (c) the subject performing a T-pose with the exoskeleton.

exoskeleton. This design accomplishes the goals of having a work-space similar to that of a healthy shoulder and being ergonomically friendly by having a distally located motor. This design is discussed in further detail throughout this paper.

3.2 Design

3.2.1 Hybrid DPL

A hybrid DPL mechanism is utilized in this exoskeleton to mimic the natural work-space of a healthy shoulder. This hybrid DPL is based off the work by Bouffard et al. [41]. Figure 3.5 shows how the DPL can rotate around a center of rotation (CR). In figure
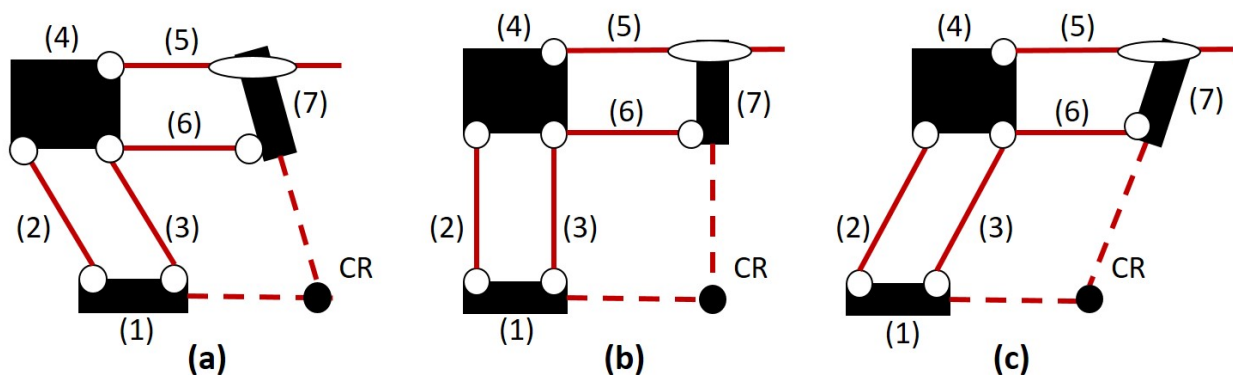
Figure 3.5. The hybrid double parallel linkage mechanism following the (a) external, (b) neutral, and (c) internal rotation of a shoulder.

3.5, link 1 and 7 represent the attachment to the backpack and the end effector respectively. Two parallelograms (1-2-3-4 and 4-5-6-7) are connected at link 4 and allow the mechanism to rotate around a fixed point. This design is considered to be a hybrid DPL because instead of a pin connecting link 5 and 7, there is a sliding joint. This sliding joint allows the position of the CR to change. The work-space of a normal DPL was calculated by Christensen et al. [2]. They determined that the DPL rotates around a fixed center of rotation, similar to that of the shoulder joint performing internal and external rotation. However, their design can only rotate with a set radius. This hybrid DPL design is capable of adjusting this radius, therefore allowing the end effector to operate in a larger work-space.

3.2.2 Exoskeleton Body and Structure

The exoskeleton mounted onto an ALICE frame backpack can be seen in figure 3.6a. An ALICE frame was chosen so that the weight of the exoskeleton could be transferred to the wearer's hips. The hybrid DPL and several structural components were 3D printed using PLA as a material. The entire exoskeleton has 4 passive degrees of freedom (DOF) and 1 active DOF. Abduction, adduction, internal and external rotation of the shoulder are passive movements while flexion and extension of the shoulder can be actively controlled by the exoskeleton. The exoskeleton is mounted to the ALICE backpack via a pin support. The pin support is composed of a 3D printed exterior with an aluminum rod inserted through its core. This reduces any deflection in the mount from the exoskeleton. The mount is in conjunction with a prismatic rail which allows the exoskeleton to be adjusted on the wearer. Figure 3.6b shows how the exoskeleton is mounted onto the backpack. It can also be seen that the motor is distally located from the arm and it is situated on the backpack.
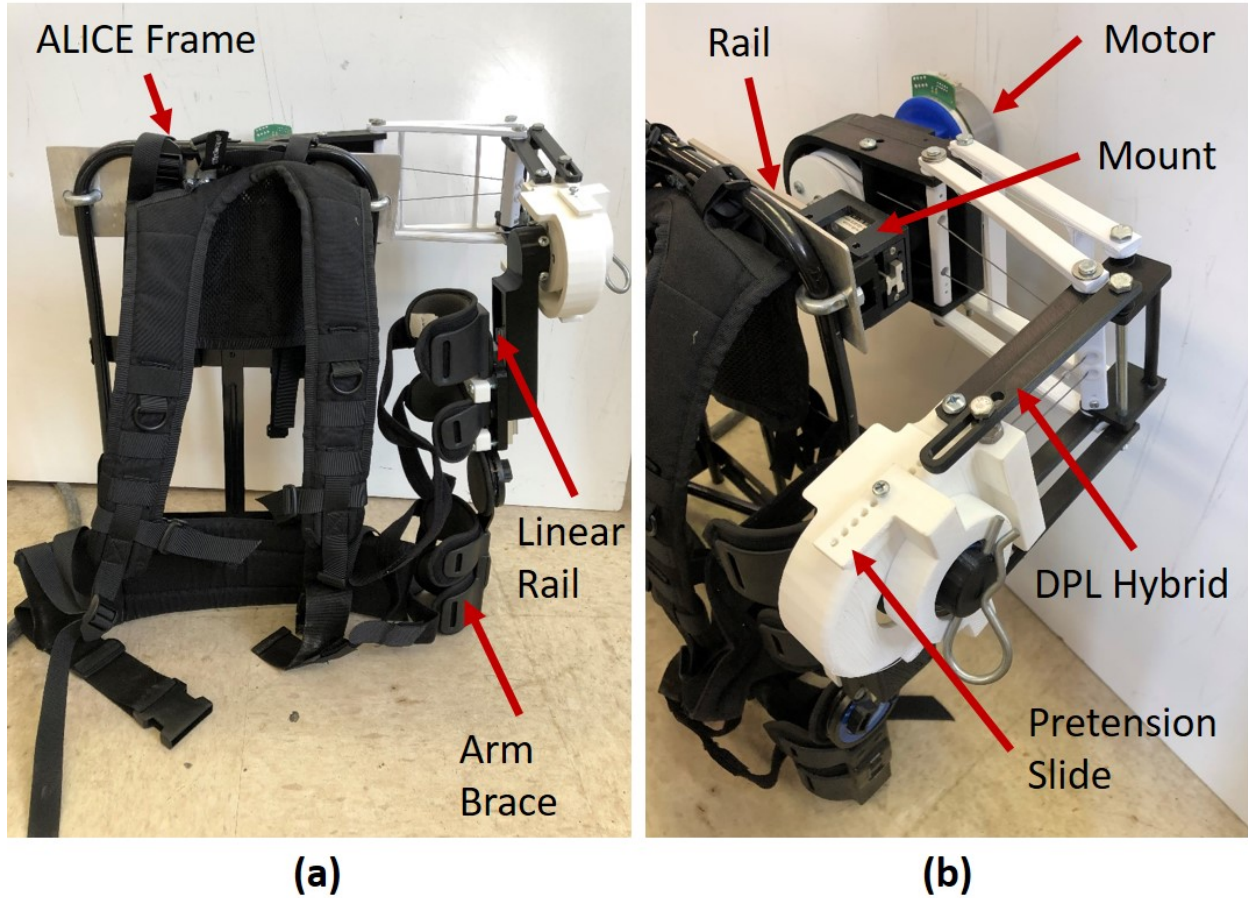
Figure 3.6. The (a) front and (b) side view of the exoskeleton mounted on the backpack.

3.2.3 Pulley System

Since the motor is distally located from the arm, torque from the motor is transferred to the arm through a pulley system. The pulley system is integrated into the hybrid DPL through the use of constraint-points. By using constraining points the cable is directed parallel to the DPL linkages and will not collide with another point. These points also keep the cable on the input and output shafts. Figure 3.7 shows the pulley system. The pulley system connects the motor shaft to an output shaft connected to the arm brace (OR092-L,Orthomen,CA, USA). In between the output shaft and arm brace are two linear rails. The combination of the linear rails and arm brace allows the torque to be transferred from the output shaft with minimal misalignments.
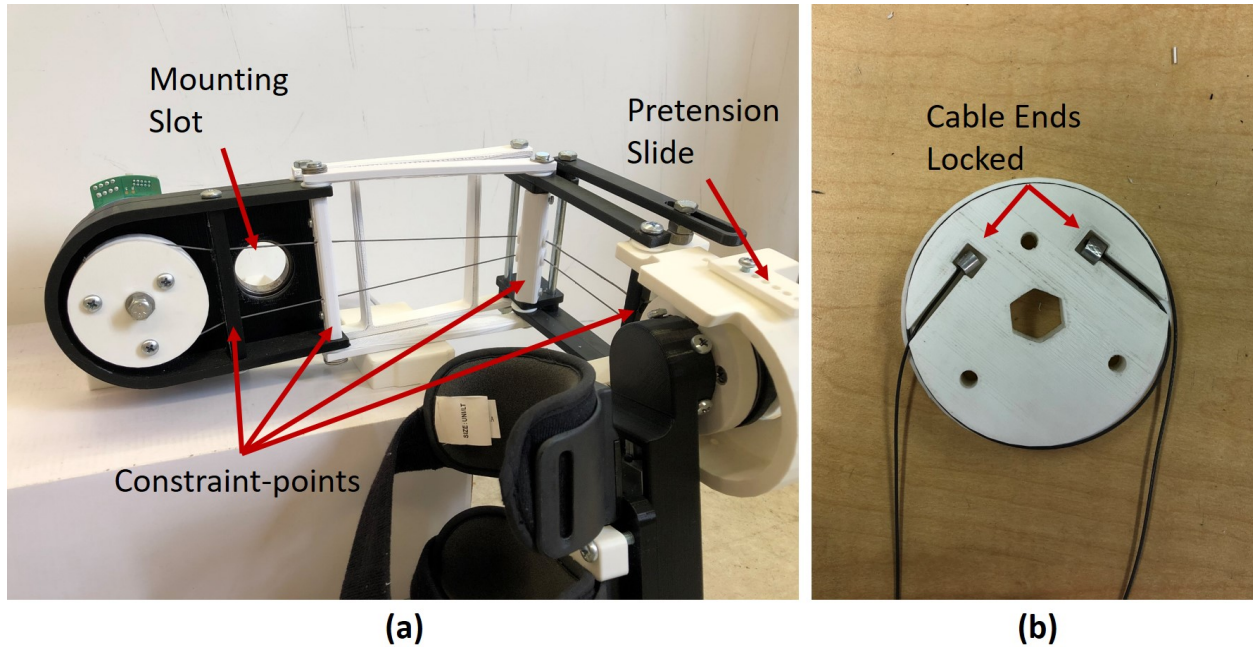
Figure 3.7. The (a) pulley system of the exoskeleton and (b) the internal geometry of the shafts.

Figure 3.8 shows how the the addition of the linear rails helps prevent any restrictions of the arm. The exoskeleton connected to an arm at rest is shown in figure 3.8a. In this system there are three points of interst at O_s (center of rotation of the shoulder), O_{exo} (center of rotation of the exoskeleton), and O_c (connection point of the exoskeleton to the arm). The origin of each point is connected by an imaginary line. For this system connecting the origins to each other creates a triangle. There are two fixed lengths in this system. They are the distances between O_s and O_c, and O_s and O_{exo}. These distances are represented in figure 3.8a. These distances are known to be fixed because neither the position of O_{exo} or the length of the arm (distance a) will change when shoulder rotation occurs. However, the distance between O_{exo} and O_c, marked as distance d, will change due to the fixed lengths of a and b. Distance d needs to change to avoid restricting arm movement. Figure 3.8b shows that as the arm moves, distance d will increase or decrease by δ due to the shift in the position of O_c. Figure 3.8c shows the neutral and rotated geometries from figure 3.8a,b superimposed. Dark green represents the arm in a neutral
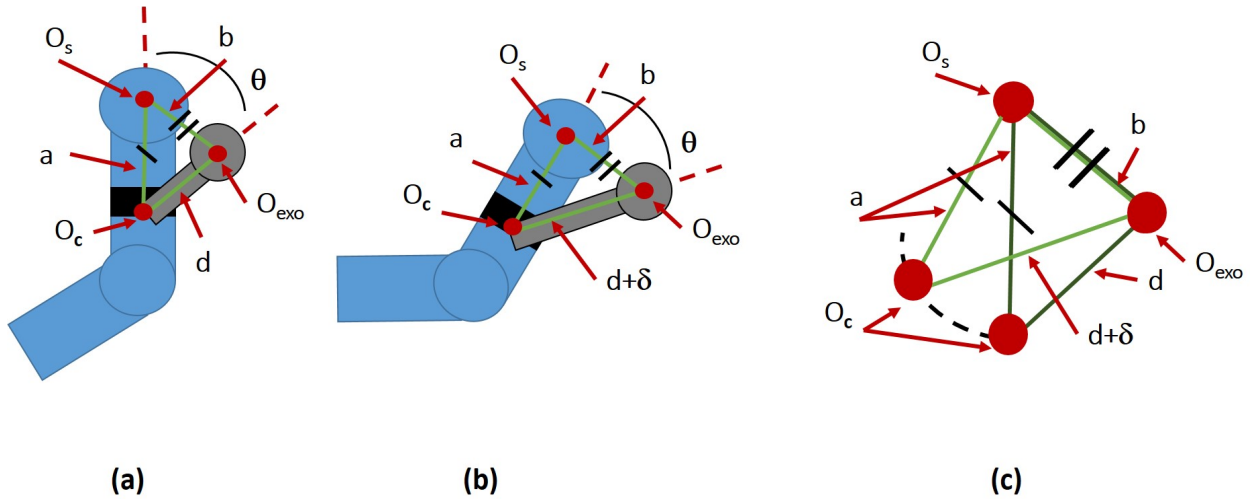
Figure 3.8. The exoskeleton connected to (a) an arm at rest, (b) an arm performing flexion, and (c) the two resulting alignment geometries of the shoulder and exoskeleton.

position. As the arm rotates the distance between O_{exo} and O_c increases to maintain a closed geometry. Thus the exoskeleton's connection to the arm must be able to account for this change in distance. The linear rails designed between the arm brace and pulley system allows for this change in distance d. In addition, the linear rails also allow the wearer to shrug.

It can be seen in figure 3.6a that the pulley system utilizes an input and output shaft. In order to secure the cable to the shaft, aluminum sleeves were crimped onto the cable and locked into the internal geometry of the motor shaft. The internal geometry of the shafts are shown in figure 3.7b. The position of the output shaft can be adjusted using the pretension slide as seen in figures 3.6 and 3.7a. The pretension slide allows the output shaft to move, which then either adds or releases tension in the cable.

3.2.4 Ergonomics

The exoskeleton was designed to be ergonomically friendly for the wearer by distally locating the motor on the backpack. The entire system weighs 6.08 kg which is less than 10% of the body weight of an average adult. It was found in literature that loads greater

than 10% of the wearer's body weight created changes in gait [35, 36, 37]. Without the ALICE frame backpack the exoskeleton weighs 3.28 kg. However, through the use of a pin support the distally located motor is capable of offsetting 73% of this weight so that the wearer only feels 0.9 kg on their arm. Using SolidWorks (Dassault Systems, MA,USA) the center of mass can be approximately located under the motor along the spinal cord. This position of center of mass has been observed to produce less discomfort to wearers [36]. In addition, the exoskeleton has several safety features. The motor and pulley system are backwards drive-able. This means that when no power is sent to the motor, the wearer can move their arm with the exoskeleton to avoid any uncomfortable positions. Hard stops were also designed into the flexion and extension movement of the arm to avoid hyper-extension or hyper-flexion.

3.2.5 Hardware and Electronics

The exoskeleton utilizes a Maxon (Maxon Precision Motors Inc.,CH) EC 90 brushless motor in series to a 10:1 planetary gearbox (Vex Robotics,TX,USA) to generate up to 10 N-m of torque to the pulley. The motor is controlled with an EPOS4 driver (EPOS4 70/15, Maxon Precision Motors Inc., CH) and a raspberry pi 4 (Raspberry Pi Foundation, UK) with a custom code. Figure 3.9 shows how the driver and raspberry pi are positioned on the ALICE backpack. The motor driver and raspberry pi are secured to the backpack with velcro zip ties. This allows the positioning of each to be very modular. The custom code uses the EPOS Command Library from Maxon to send positional commands directly to the driver. The exoskeleton uses an open loop control system configuration.

3.3 Forward Kinematics

A basic model of the exoskeleton was created and can be seen in figure 3.10. From this model the Denavit-Hartenberg (DH) parameters were extracted to be used to calculate the work-space of the exoskeleton. Table 3.1 displays the DH parameters.
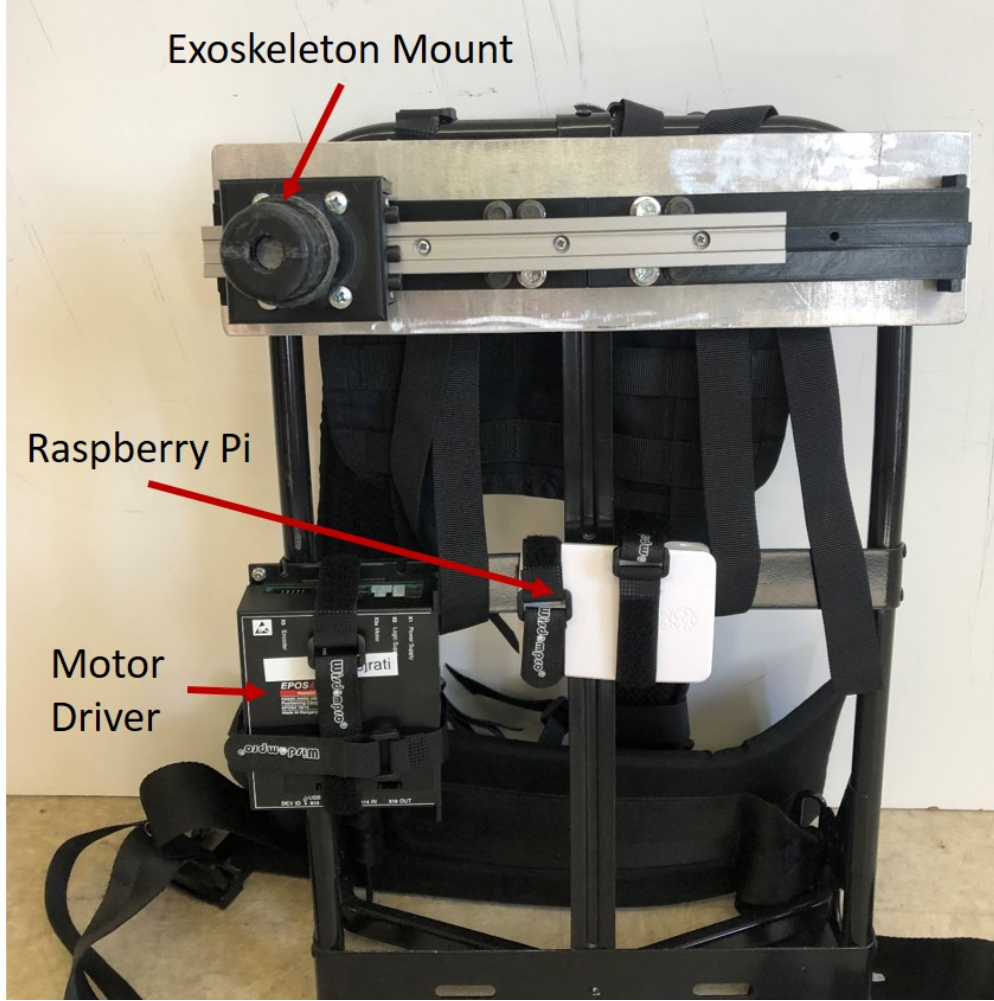
Figure 3.9. The positioning of the motor driver and raspberry pi on the ALICE backpack.

Table 3.1. DH parameters for the exoskeleton; lengths are in m.

i	a	d	α	θ
1	0.04	0	$-\pi/2$	$0° \leq \theta_1^* \leq 90°$
2	0.15	0	0	$-58° \leq \theta_2^* \leq 58°$
3	0.10	0	0	$X_3 \leq \theta_3^* \leq$ -75.7°
4	0.08	0	$\pi/2$	θ_4^*
5	0.16	0	0	$-50° \leq \theta_5^* \leq 160°$

The first DOF was θ_1 which performs adduction and abduction of the arm. This is a passive DOF. For the forward kinematic calculations, the range of motion of θ_1 was restricted from 0 to 90°. This was selected because this is the area that the exoskeleton will primarily operate. θ_2 represented the first DOF of the hybrid DPL. This is also a passive DOF. Using a SolidWorks model, the ROM of this joint was determined to be between -58
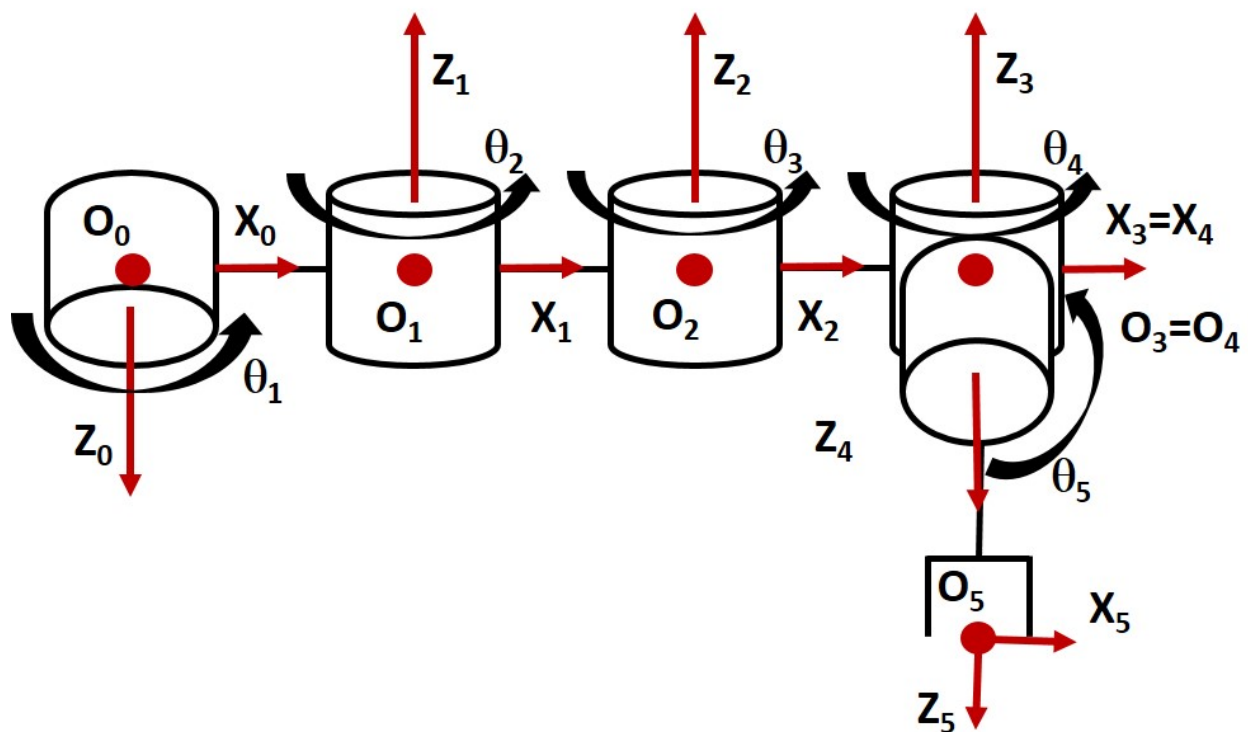
Figure 3.10. Zero angle model (front view) of the exoskeleton.

to 58°. It was also determined that the ROM of θ_3 was dependent on θ_2. More specifically, the minimum value θ_3 could rotate depended the position of θ_2. This minimum limit is denoted as X_3 in table 3.1. An equation was then computed using Solidworks to define the relationship between X_3 and θ_2. Equation 3.1 shows this relationship. This equation has an adjusted R^2 value of 0.94.

$$X_3 = 1.06E^{-5}\theta_2^3 + 0.005\theta_2^2 + 0.27\theta_2 - 120.8 \qquad (3.1)$$

Where:

X_3 is the minimum limit for the ROM of theta 3

θ_2 is the angle of theta 2

For simplification, the effects of θ_4 are considered to be zero because it is primarily used to attach the arm brace to the wearer. This is another passive DOF. θ_5 is an active DOF which is controlled by the motor and pulley system. For calculations, the ROM of this DOF is from -50 to 160°. Using these DH parameters, the forward kinematics were computed using a custom code in MATLAB with the following equations:

$$^{i-1}R_i = R_{z_{i-1}}(\theta)R_{x_i}(\alpha) \tag{3.2}$$

$$^{i-1}d_{i-1,i} = \sum_{i=1}^{i} {}^{i-1}R_i a_i{}^i x_i + d_i{}^{i-1} z_{i-1} \tag{3.3}$$

$$^{0}d_{0n} = \sum_{n=1}^{n} {}^{0}d_{n-1,n} \tag{3.4}$$

Where:

R is a rotation matrix

θ is the rotation about the z-axis

α is the rotation about the x-axis

d is a distance with respect to another point

a is the distance along the x-axis

These equations computed the rotation matrices, positional vectors, and the sum of these vectors. This allowed for the computation of the position of the end effector with respect to the origin as each DOF moved. The computed work-space of the exoskeleton can be seen in figure 3.11. The red dots seen in figure 3.11 represent the points the exoskeleton can reach. These points were calculated using the MATLAB code. As it can be seen, the exoskeleton is capable of mimicking the work-space of a shoulder. The hybrid DPL allows
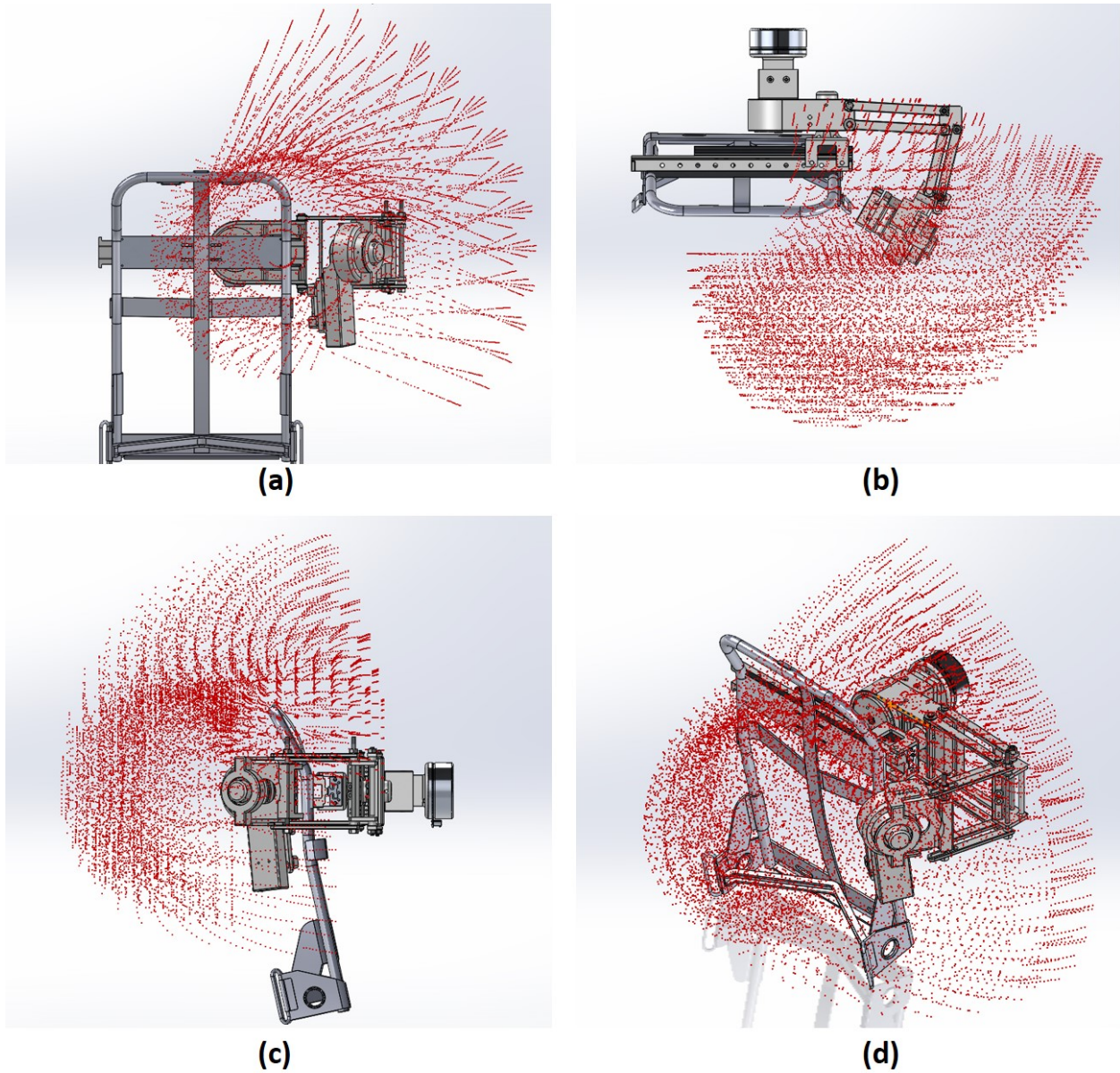
Figure 3.11. Work-space of the exoskeleton as seen in the (a) frontal plane, (b) transverse plane, (c) sagittal plane, and (d) from an isotropic view.

the exoskeleton to rotate around an unfixed CR. This allows for increased movement in the transverse plane as seen in figure 3.11b.

3.4 Experimental Procedure and Setup

3.4.1 Experimental Setup

Figure 3.12a shows the experimental setup used to verify the exoskeleton's ability to generate arm swing. The setup consists of a 1 DOF shoulder joint which is attached to a passive dummy arm. The dummy arm weighs 1.95 kg which is around the same weight as half the average combination of an arm and hand [42]. Two IMUs (XSENS DOT,XSENS, NL) were used to capture the rotation of the motor shaft and of the dummy arm at a sampling rate of 60 Hz.

3.4.2 Experimental Procedure

Two testing conditions were performed to test the exoskeleton's ability to generate arm swing. The first condition involved the dummy arm swinging in-plane which simulates a person swinging their arm strictly in the sagittal plane. This can be seen in figure 3.12b. For the second condition, the dummy arm swung out-of-plane to simulate arm swing across the front of the body. Figure 3.12c shows the out-of-plane condition. The arm is rotated internally 25° for this condition.
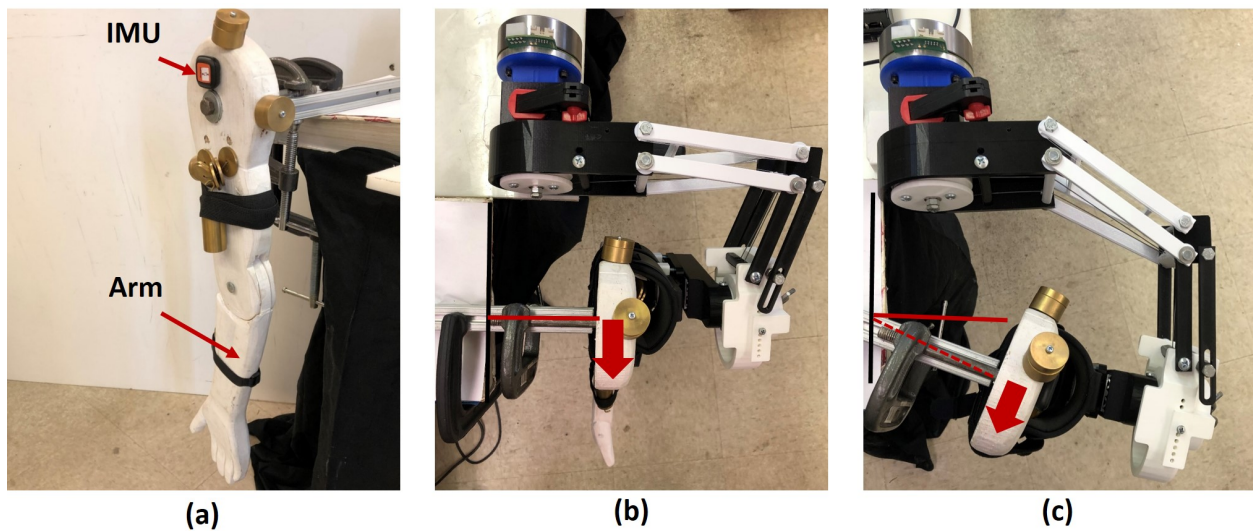
Figure 3.12. The (a) passive arm with the arm swing (b) in-plane and (c) out-of-plane.

For both conditions, the motion of the dummy arm was observed. The motor input an amplitude of $\pm25°$ to the system at frequencies of 0.67, 0.8, and 1.1 Hz. The exoskeleton was tested with a range of motion (ROM) of 50° since this is approximately double the range of motion of the shoulder joint during walking. The arm performed 20 cycles for each speed during each condition. Data was then sent to MATLAB (MathWorks Inc.) where further calculations were performed. To determine the performance of the exoskeleton, the ROM of the dummy arm was calculated. Additionally, the cross-correlation between the motion of the motor and dummy arm was computed as outlined by Chesebrough et al.[43].

3.4.3 Work-space Analysis

A work-space analysis was performed to verify the forward kinematics shown in the Forward Kinematics section. Tracker, a 2D motion capture software, was used to track the ROM of a person while they wore the device. Three conditions were performed to observe motion in the frontal, sagittal, and transverse planes. The first condition involved the subject performing flexion and extension of the arm. Next the subject performed abduction and adduction of the arm. Lastly, the subject performed internal and external rotation of
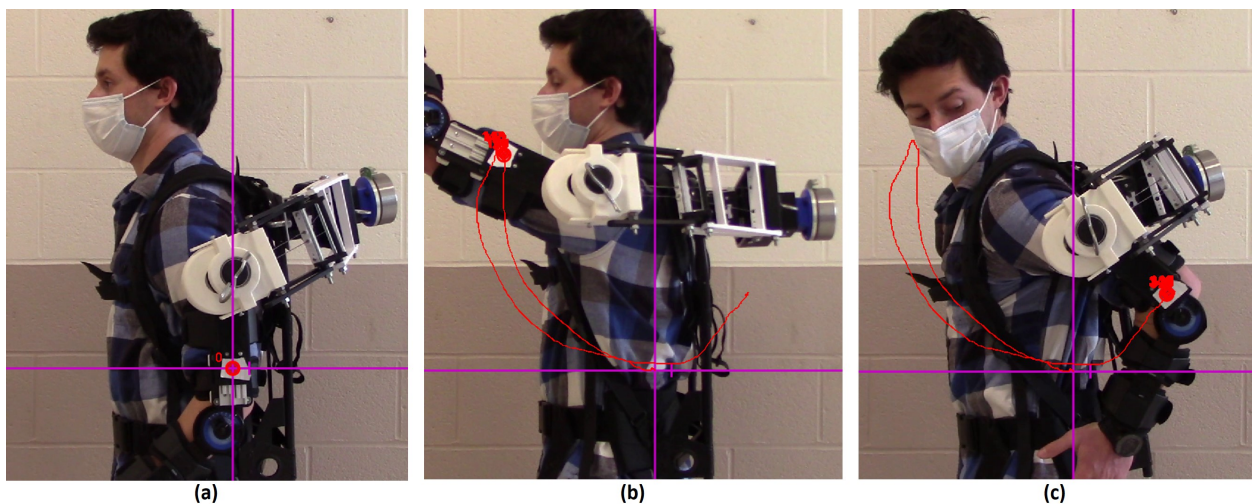
Figure 3.13. The arm being tracked while (a) at rest, (b) performing flexion, and (c) performing extension.

38

the shoulder. An example of the motion of the arm being tracked is seen in figure 3.13. Once collected, the data was then exported from Tracker to MATLAB for further analysis.

3.5   Results and Discussion

3.5.1   Arm Swing Analysis

Figure 3.14 shows the results from the exoskeleton generating arm swing on the dummy arm. For figure 3.14, 0° refers to the arm at rest. The cross-correlation between the motion of the motor and the dummy arm is displayed in table 3.2. The ROM of the dummy arm was also computed and its values are presented in table 3.3.

The exoskeleton generated arm swing at three different frequencies for both conditions. Figure 3.14a,b shows the response of the dummy arm when an input frequency of 0.67 Hz was induced. It can be seen that the ROM of the dummy arm for both conditions is around 35° which is far less than the input ROM of 50°. However, despite a lack of ROM, the dummy arm is very responsive to changes in the direction of the motor. This can be seen in the high cross-correlation value of -0.99 with low time lags. It should be noted that the negative sign only indicates that positive rotation of the motor induces a negative rotation in the dummy arm due to the right hand rule.

Similar behavior is seen when the dummy arm rotates at a frequency of 0.80 Hz. These results can be seen in figure 3.14c,d. The correlation between the motor and the arm remains at -0.99 with minimal time lag. This indicates that the dummy arm will respond to inputs from the motor regardless of the input frequency. However, the ROM of the dummy arm increases as seen in table 3.3. Again, both the in-plane and out-of-plane conditions have similar ROM. At 0.80 Hz the ROM is approaching the desired 50° of ROM. This is likely because the exoskeleton can generate more momentum at this frequency which translates to more movement in the dummy arm.

The last frequency at which the dummy arm was tested at was 1.10 Hz. The motion of the dummy arm can be seen in figure 3.14e,f. At this frequency the ROM observed during
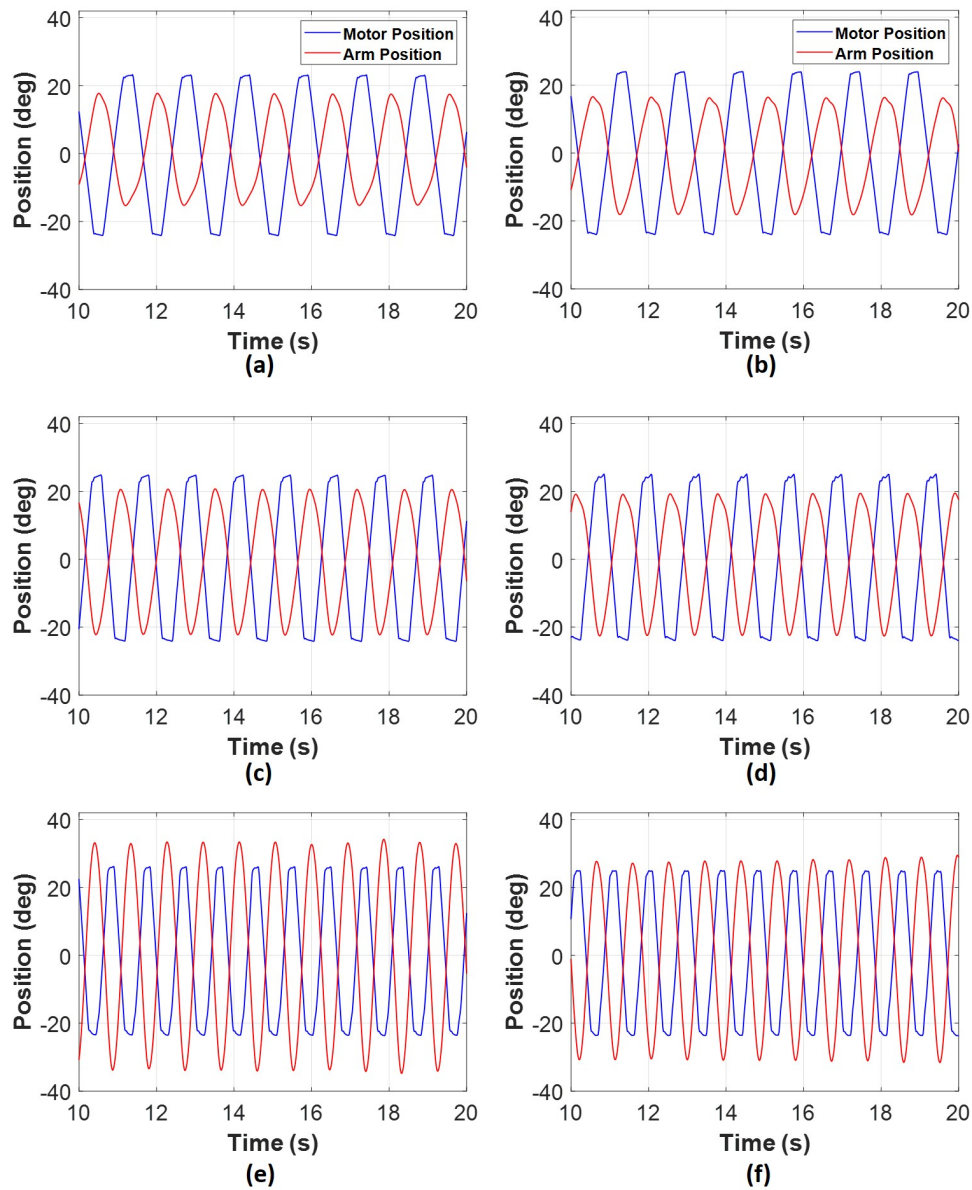
Figure 3.14. Arm motion in-plane (first column) and out-of-plane (second column) at (a)(b) 0.67 Hz, (c)(d) 0.80 Hz, and 1.10 Hz (e)(f) respectively.

both conditions begin to diverge. The in-plane condition experienced a ROM of 69.6° and a ROM of 63.2° was observed during the out-of-plane condition. Both of these ROM overshoot the desired 50° which further indicates that at higher frequencies, the exoskeleton is able to generate more momentum in the dummy arm. Despite overshooting the target ROM, the exoskeleton still produces highly correlated movements between the

Table 3.2. Cross-correlation analysis between the motor movements and the passive arm.

| | In-plane | | Out-of-Plane | |
Frequency	Cross-correlation	Time lag (s)	Cross-correlation	Time lag (s)
0.67 Hz	-0.99	-0.03	-0.99	-0.02
0.80 Hz	-0.99	-0.02	-0.99	-0.03
1.10 Hz	-0.99	-0.05	-0.99	-0.05

Table 3.3. Range of Motion for the in-plane and out-of-plane passive arm.

| | Range of Motion | |
Frequency	In-plane	Out-of-plane
0.67 Hz	34.8°	35.2°
0.80 Hz	43.7°	43.6°
1.10 Hz	69.6°	63.2°

dummy arm and the motor. This further indicates that the exoskeleton can induce highly correlated movements despite the input frequency.

The torque at each frequency and condition were calculated using equation 3.5. The mass moment of inertia was calculated by replicating the dummy arm in SolidWorks and utilizing material properties to determine the mass moment of inertia. The mass moment of inertia about the center of rotation had a value of 0.1172 kg-m^2.

$$T = I\alpha + mglsin(\theta) \tag{3.5}$$

Where:

T is torque

I is the mass moment of inertia

α is angular acceleration

m is mass

g is gravity
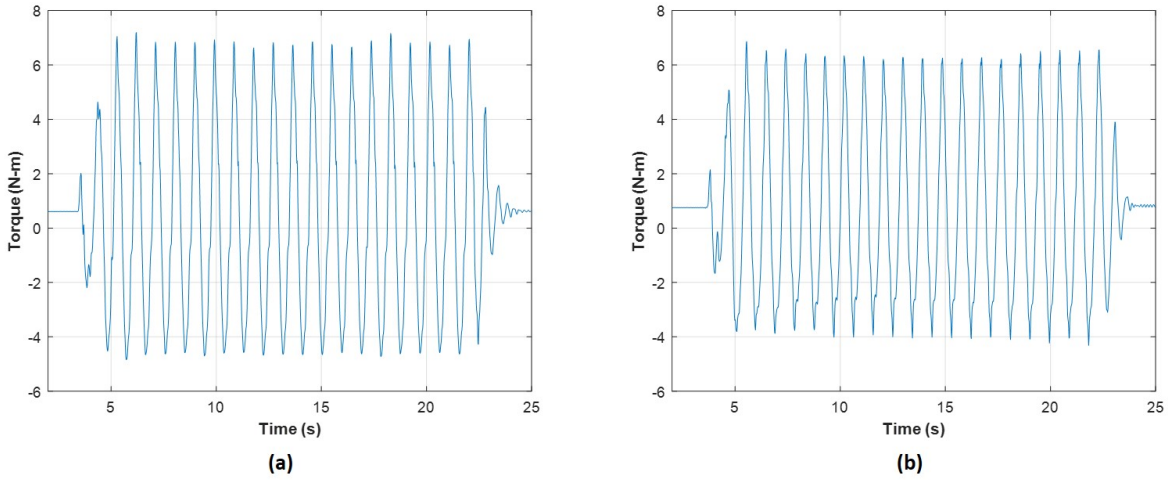
Figure 3.15. Calculated torque at the 1.10 Hz frequency for the (a) in-plane and (b) out-of-plane conditions.

l is the distance from the origin of rotation to the center of mass

θ is the angle of rotation

The computed torques can be seen in table 3.4. It is observed that the maximum torques occurred at the frequency of 1.10 Hz with the maximum occurring in the in-plane condition. The torque profiles at this frequency can be seen in figure 3.15. These torque values indicate that the exoskeleton is capable of generating a large amount of torque, regardless of the orientation of the shoulder.

The exoskeleton's ability to generate arm swing was then tested on two human subjects. The goal of this was to determine if the subjects would react to the torque from the exoskeleton. The subjects did not resist the exoskeleton's motion, but moved their arm

Table 3.4. Computed maximum torque for the in-plane and out-of-plane passive arm.

| | Generated Torque | |
Frequency	In-plane	Out-of-plane
0.67 Hz	2.65 N-m	3.19 N-m
0.80 Hz	4.38 N-m	4.53 N-m
1.10 Hz	7.19 N-m	6.87 N-m

42
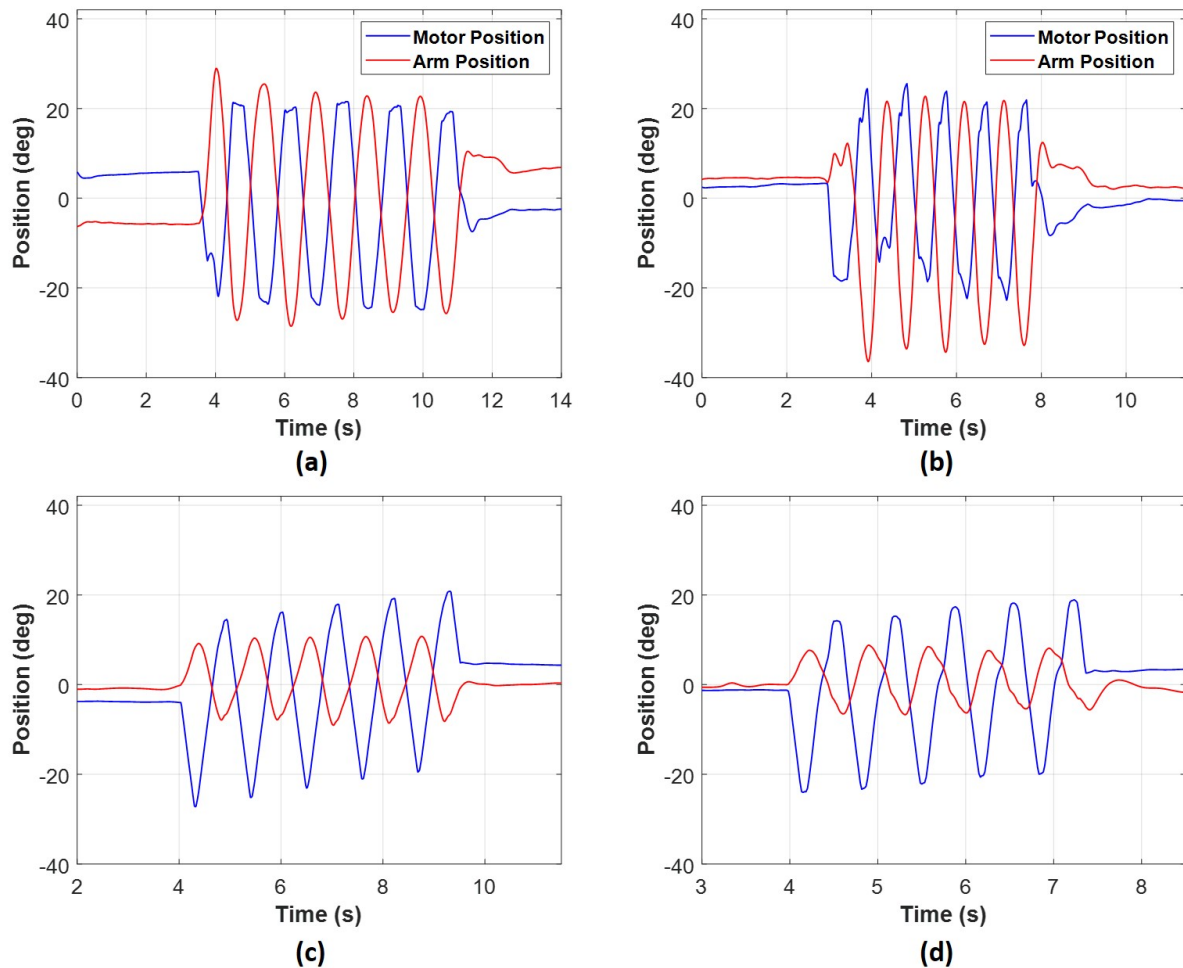
Figure 3.16. The first subject's response to the exoskeleton at frequencies of (a) 0.67 and (b) 1.10 Hz and the second subject's response to the exoskeleton at frequencies of (c) 0.90 Hz and (d) 1.40 Hz.

with the exoskeleton when prompted. Figure 3.16 shows the results. The first subject was tested at frequencies of 0.67 and 1.10 Hz. It was observed that the subject responded to the exoskeleton at both frequencies. The cross correlation between the subject's arm movements and the motor shaft was computed. High cross correlations existed between the arm and motor shaft position. At 0.67 and 1.10 Hz, there were cross correlation coefficients of -0.98 and -0.93 respectively with low time lags. Subject two was then tested at 0.90 Hz and 1.40 Hz as seen in figure 3.16c,d. It was found that the cross correlation coefficients

Table 3.5. Range of motion while wearing the exoskeleton.

Movement	Range	Exoskeleton	Overlap
Flexion	170°	144.89°	85.23%
Extension	-60°	-50.39°	83.99%
Abduction	120°	171.5°	100.00%
Adduction	-20°	-64.81°	100.00%
External	90°	30.15°	33.50%
Internal	-60°	-85.91°	100.00%

were -0.95 and -0.94 respectively. Low time lags were also observed. These high correlation coefficients indicate that the subjects responded quickly to a change in direction of the exoskeleton, similar to arm swing during walking. This proves that the exoskeleton can induce arm swing at a desired frequency.

3.5.2 Work-space Analysis

A work-space analysis was performed to validate the forward kinematics calculations above. This was done by tracking the arm motion of a subject while they wore the device. Table 3.5 shows the ROM of a subject while they wore the exoskeleton. The observed motion of the shoulder joint was then compared to a natural ROM of a shoulder joint as outlined in literature [2]. The work-space of the subject highly overlaps with that of a natural shoulder joint. It can be seen that when the subject is wearing the exoskeleton, they can flex their shoulder 145° and also extend the shoulder -50°. These values overlap approximately 84% with that of a natural shoulder. For both abduction and adduction the subject could rotate past the goal values indicating that the shoulder girdle began to rotate as well. However, this shows that the device allows the shoulder to reach 120° and -20°. For external rotation of the shoulder, the device restricted the subject and only allowed the subject to rotate 33% of the desired ROM. Although this is low, this is still sufficient for the desired use of this exoskeleton which is to induce arm swing in the wearer. Internal and external rotation during walking is small. Future work will include resizing the linkages to allow the wearer to perform more internal shoulder rotation.
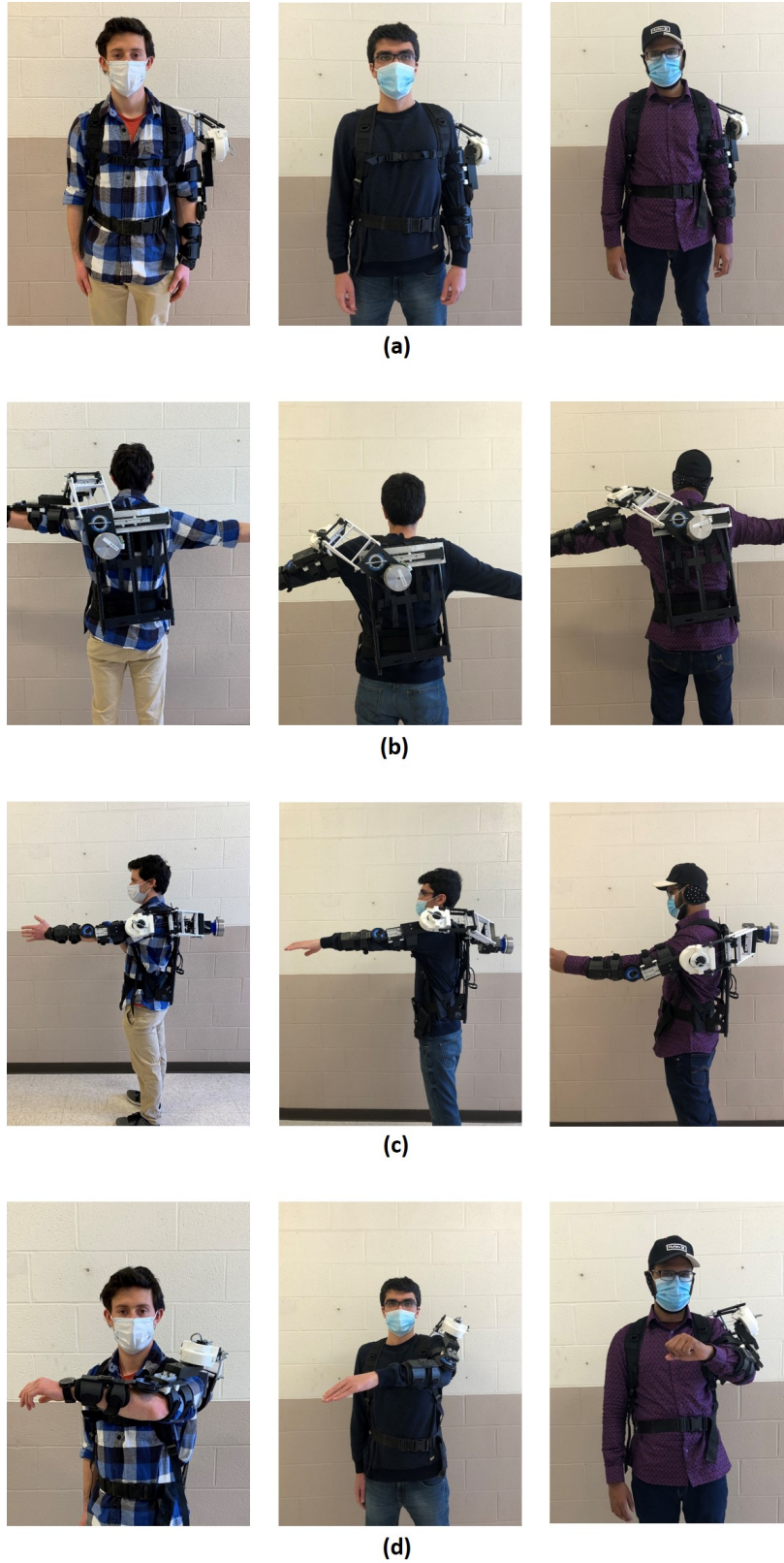
Figure 3.17. Three subjects wearing the exoskeleton in a (a) relaxed position, (b) T-pose, (c) shoulder flexion, and (d) reaching across their bodies.

To verify that multiple people could wear the exoskeleton, three subjects wore the device and performed four positions. The subject's heights ranged from 1.65-1.83 m (1.75 ± 0.09 m) reported as (mean ± standard deviation). Figure 3.17 displays the subjects performing the four movements. For the fist movement, subjects was placed their arms in a relaxed position next to their hips. This position was achieved easily. Next, the subjects performed a T-pose as seen in figure 3.17b. The subjects had no issues with this pose. Then subjects flexed their arms, reaching out in front of their bodies. The last position involved the subjects reaching across their bodies as seen in figure 3.17d. This position was slightly harder to perform for one subject due to a restriction in the internal rotation of their shoulder. This restricted their ability to reach across their body. However, this was achieved more easily by the other two subjects. These positions verify that multiple people can wear the exoskeleton. Some future work will include manufacturing larger and more robust linkages so that internal rotation of the shoulder is less restricted.

3.6   Conclusion

A novel distally located upper extremity exoskeleton was presented in this chapter. The purpose of this device is to induce arm swing in the wearer while allowing natural movements of the shoulder. The exoskeleton utilizes a hybrid DPL mechanism to mimic the work-space of a natural shoulder. By distally locating the motor the device's overall ergonomics are improved.

The exoskeleton's work-space and ability to generate arm swing was validated through two experimental procedures. The exoskeleton was tested on a passive dummy arm and the motion of the arm was observed. In addition, the device was worn on a human subject and the ROM of the subject wearing the exoskeleton was compared to that of a normal shoulder joint. It was discovered that the device can induce highly correlated movements in the passive arm regardless of the input frequency. Also, the exoskeleton is capable of overlapping a high percentage of a shoulder joint's work-space.

Future work on the exoskeleton includes developing a closed loop control system for the motor to provide more accurate positional commands. In addition, larger linkages need to be manufactured using a stronger material than PLA. This will help reduce any deflections and allow for a larger work-space for the exoskeleton to operate. Based on these findings, this exoskeleton has the potential to help rehabilitate arm swing for gait rehabilitation.

REFERENCES

[1] Cui, X., Chen, W., Jin, X., and Agrawal, S. K., 2016. "Design of a 7-dof cable-driven arm exoskeleton (carex-7) and a controller for dexterous motion training or assistance". *IEEE/ASME Transactions on Mechatronics,* **22**(1), pp. 161–172.

[2] Christensen, S., and Bai, S., 2018. "Kinematic analysis and design of a novel shoulder exoskeleton using a double parallelogram linkage". *Journal of Mechanisms and Robotics,* **10**(4).

[3] Jones, M., Bouffard, C., and Hejrati, B., 2019. "A shoulder mechanism for assisting upper arm function with distally located actuators". In 2019 41st Annual International Conference of the IEEE Engineering in Medicine and Biology Society (EMBC), IEEE, pp. 6233–6236.

[4] Collins, S. H., Adamczyk, P. G., and Kuo, A. D., 2009. "Dynamic arm swinging in human walking". *Proceedings of the Royal Society B: Biological Sciences,* **276**(1673), pp. 3679–3688.

[5] Behrman, A. L., and Harkema, S. J., 2000. "Locomotor training after human spinal cord injury: a series of case studies". *Physical therapy,* **80**(7), pp. 688–700.

[6] Elftman, H., 1939. "The function of the arms in walking". *Human biology,* **11**(4), p. 529.

[7] Ferris, D. P., Huang, H. J., and Kao, P.-C., 2006. "Moving the arms to activate the legs". *Exercise and sport sciences reviews,* **34**(3), pp. 113–120.

[8] Sylos-Labini, F., Ivanenko, Y. P., MacLellan, M. J., Cappellini, G., Poppele, R. E., and Lacquaniti, F., 2014. "Locomotor-like leg movements evoked by rhythmic arm movements in humans". *PloS one,* **9**(3).

[9] Kaupp, C., Pearcey, G. E., Klarner, T., Sun, Y., Cullen, H., Barss, T. S., and Zehr, E. P., 2018. "Rhythmic arm cycling training improves walking and neurophysiological integrity in chronic stroke: the arms can give legs a helping hand in rehabilitation". *Journal of neurophysiology,* **119**(3), pp. 1095–1112.

[10] Gassert, R., and Dietz, V., 2018. "Rehabilitation robots for the treatment of sensorimotor deficits: a neurophysiological perspective". *Journal of neuroengineering and rehabilitation,* **15**(1), pp. 1–15.

[11] Wu, Y., Li, Y., Liu, A.-M., Xiao, F., Wang, Y.-Z., Hu, F., Chen, J.-L., Dai, K.-R., and Gu, D.-Y., 2016. "Effect of active arm swing to local dynamic stability during walking". *Human movement science,* **45**, pp. 102–109.

[12] Hejrati, B., Chesebrough, S., Foreman, K. B., Abbott, J. J., and Merryweather, A. S., 2016. "Comprehensive quantitative investigation of arm swing during walking at various speed and surface slope conditions". *Human movement science,* **49**, pp. 104–115.

[13] Tester, N. J., Barbeau, H., Howland, D. R., Cantrell, A., and Behrman, A. L., 2012. "Arm and leg coordination during treadmill walking in individuals with motor incomplete spinal cord injury: a preliminary study". *Gait & posture,* **36**(1), pp. 49–55.

[14] Huang, X., Mahoney, J. M., Lewis, M. M., Du, G., Piazza, S. J., and Cusumano, J. P., 2012. "Both coordination and symmetry of arm swing are reduced in parkinson's disease". *Gait & posture,* **35**(3), pp. 373–377.

[15] Hejrati, B., Merryweather, A. S., and Abbott, J. J., 2017. "Generating arm-swing trajectories in real-time using a data-driven model for gait rehabilitation with self-selected speed". *IEEE Transactions on Neural Systems and Rehabilitation Engineering,* **26**(1), pp. 115–124.

[16] Ford, M. P., Wagenaar, R. C., and Newell, K. M., 2007. "The effects of auditory rhythms and instruction on walking patterns in individuals post stroke.". *Gait & posture,* **26**(1), jun, pp. 150–5.

[17] Stephenson, J. L., Lamontagne, A., and De Serres, S. J., 2009. "The coordination of upper and lower limb movements during gait in healthy and stroke individuals". *Gait & posture,* **29**(1), pp. 11–16.

[18] Krasovsky, T., Lamontagne, A., Feldman, A. G., and Levin, M. F., 2013. "Reduced gait stability in high-functioning poststroke individuals". *Journal of neurophysiology,* **109**(1), pp. 77–88.

[19] De Graaf, M. L., Hubert, J., Houdijk, H., and Bruijn, S. M., 2019. "Influence of arm swing on cost of transport during walking". *Biology open,* **8**(6), p. bio039263.

[20] Pontzer, H., Holloway, J. H., Raichlen, D. A., and Lieberman, D. E., 2009. "Control and function of arm swing in human walking and running". *Journal of Experimental Biology,* **212**(4), pp. 523–534.

[21] Goudriaan, M., Jonkers, I., van Dieen, J. H., and Bruijn, S. M., 2014. "Arm swing in human walking: What is their drive?". *Gait & posture,* **40**(2), pp. 321–326.

[22] Canton, S., and MacLellan, M. J., 2018. "Active and passive contributions to arm swing: Implications of the restriction of pelvis motion during human locomotion". *Human movement science,* **57**, pp. 314–323.

[23] Kuhtz-Buschbeck, J. P., and Jing, B., 2012. "Activity of upper limb muscles during human walking". *Journal of Electromyography and Kinesiology,* **22**(2), pp. 199–206.

[24] Yegian, A. K., Tucker, Y., Gillinov, S., and Lieberman, D. E., 2019. "Straight arm walking, bent arm running: gait-specific elbow angles". *Journal of Experimental Biology,* **222**(13), p. jeb197228.

[25] Koo, H.-M., and Lee, S.-Y., 2016. "Gait analysis on the condition of arm swing in healthy young adults". *Physical Therapy Rehabilitation Science,* **5**(3), pp. 149–154.

[26] Chen, T., Casas, R., and Lum, P. S., 2019. "An elbow exoskeleton for upper limb rehabilitation with series elastic actuator and cable-driven differential". *IEEE Transactions on Robotics,* **35**(6), pp. 1464–1474.

[27] Klein, J., Spencer, S., Allington, J., Minakata, K., Wolbrecht, E., Smith, R., Bobrow, J., and Reinkensmeyer, D., 2008. "Biomimetic orthosis for the neurorehabilitation of the elbow and shoulder (bones)". In 2008 2nd IEEE RAS & EMBS international conference on biomedical robotics and biomechatronics, IEEE, pp. 535–541.

[28] Trigili, E., Crea, S., Moisè, M., Baldoni, A., Cempini, M., Ercolini, G., Marconi, D., Posteraro, F., Carrozza, M. C., and Vitiello, N., 2019. "Design and experimental characterization of a shoulder-elbow exoskeleton with compliant joints for post-stroke rehabilitation". *IEEE/ASME Transactions on Mechatronics,* **24**(4), pp. 1485–1496.

[29] Nef, T., and Riener, R., 2005. "Armin-design of a novel arm rehabilitation robot". In 9th International Conference on Rehabilitation Robotics, 2005. ICORR 2005., IEEE, pp. 57–60.

[30] Liu, C., Zhu, C., Liang, H., Yoshioka, M., Murata, Y., and Yu, Y., 2016. "Development of a light wearable exoskeleton for upper extremity augmentation". In 2016 23rd International Conference on Mechatronics and Machine Vision in Practice (M2VIP), IEEE, pp. 1–6.

[31] Sui, D., Fan, J., Jin, H., Cai, X., Zhao, J., and Zhu, Y., 2017. "Design of a wearable upper-limb exoskeleton for activities assistance of daily living". In 2017 IEEE International Conference on Advanced Intelligent Mechatronics (AIM), IEEE, pp. 845–850.

[32] Hsieh, H.-C., Chien, L., and Lan, C.-C., 2015. "Mechanical design of a gravity-balancing wearable exoskeleton for the motion enhancement of human upper limb". In 2015 IEEE International Conference on Robotics and Automation (ICRA), IEEE, pp. 4992–4997.

[33] Lessard, S., Pansodtee, P., Robbins, A., Trombadore, J. M., Kurniawan, S., and Teodorescu, M., 2018. "A soft exosuit for flexible upper-extremity rehabilitation". *IEEE Transactions on Neural Systems and Rehabilitation Engineering,* **26**(8), pp. 1604–1617.

[34] Tsai, T.-Y., Chang, C.-Y., Chung, M.-T., Lu, K.-C., Huang, J.-F., and Shih, W.-P., 2018. "A portable exoskeleton driven by pneumatic artificial muscles for upper limb motion replication". In Proceedings of the 6th International Conference on Control, Mechatronics and Automation, pp. 133–138.

[35] Li, S. S., and Chow, D. H., 2018. "Effects of backpack load on critical changes of trunk muscle activation and lumbar spine loading during walking". *Ergonomics,* **61**(4), pp. 553–565.

[36] Chen, Y.-L., and Mu, Y.-C., 2018. "Effects of backpack load and position on body strains in male schoolchildren while walking". *PloS one,* **13**(3), p. e0193648.

[37] Devroey, C., Jonkers, I., De Becker, A., Lenaerts, G., and Spaepen, A., 2007. "Evaluation of the effect of backpack load and position during standing and walking using biomechanical, physiological and subjective measures". *Ergonomics,* **50**(5), pp. 728–742.

[38] Chaffin, D. B., Andersson, G. B., and Martin, B. J., 2006. *Occupational biomechanics.* John wiley & sons.

[39] Angelini, L., Damm, P., Zander, T., Arshad, R., Di Puccio, F., and Schmidt, H., 2018. "Effect of arm swinging on lumbar spine and hip joint forces". *Journal of biomechanics,* **70**, pp. 185–195.

[40] Umberger, B. R., 2008. "Effects of suppressing arm swing on kinematics, kinetics, and energetics of human walking". *Journal of biomechanics,* **41**(11), pp. 2575–2580.

[41] Bouffard, C., 2019. "An upper extremity exoskeleton utilizing a modified double parallelogram linkage mechanism with proximally located actuators".

[42] De Leva, P., 1996. "Adjustments to zatsiorsky-seluyanov's segment inertia parameters". *Journal of biomechanics,* **29**(9), pp. 1223–1230.

[43] Chesebrough, S., Hejrati, B., and Hollerbach, J., 2019. "The treadport: natural gait on a treadmill". *Human factors,* **61**(5), pp. 736–748.

BIOGRAPHY OF THE AUTHOR

Jacob Bloom was born in Portland, Maine. He graduated from Scarborough High School in 2015. He then attended the University of Maine at Orono for his undergraduate studies. There he received a bachelors of science in mechanical engineering with a minor in biomedical engineering and robotics. Jacob's research focuses on gait rehabilitation using arm swing. Jacob Bloom is a candidate for the Master of Science degree in Mechanical Engineering from the University of Maine in May 2021.